Cellular and Molecular Life Sciences (2025) 82:105
https://doi.org/10.1007/s00018-025-05604-0

ORIGINAL ARTICLE

IGF2BP1-HAX-1 positive feedback loop-mediated HAX-1 overexpression blocks autophagic flux and promotes chemoresistance in nasopharyngeal carcinoma

Siyu Zhang[1,2] · Miao Gu[1,2] · Haimeng Yin[1,2] · Si Pan[1,2] · Haijing Xie[1,2] · Wenhui Chen[1,2] · Sheraz Gul[3,4] · Yue Zhao[5] · Zhefang Wang[7] · Wenjie Zheng[6] · Yiwen You[1,2] · Bo You[1,2]

Received: 28 June 2024 / Revised: 10 October 2024 / Accepted: 22 January 2025

Abstract

Autophagy is associated with chemoresistance, which is the leading cause of failure in chemotherapeutic treatments. Among the various aspects of autophagy, autophagic flux serves as a critical indicator for evaluating the dynamic processes involved. We report herein that the multifunctional protein HAX-1 promotes chemoresistance by effectively blocking the fusion of autophagosomes with lysosomes. Complementary mass spectrometric and functional studies also demonstrated that HAX-1 recruits NEDD4 to promote Rab7a degradation and inhibits binding of Rab7a with SNAREs by competitively binding to it. Furthermore, HAX-1 binds IGF2BP1 mRNA, thereby contributing to its stability and translation. Moreover, IGF2BP1 enhanced HAX-1 m6A methylation, thereby enhancing its stability. By way of *in-vivo* and *in-vitro* experiments, we confirmed the positive role of the IGF2BP1-HAX-1 feedback loop in chemoresistance. Taken together, our findings provide evidence that monitoring of HAX-1, IGF2BP1, and SQSTM1 levels can serve as useful predictors of clinical outcome and chemoresistance risk. In addition, our data provide new insights into the clinical applications of therapies related to autophagic flux and its associated molecular network in targeting cisplatin chemoresistance in nasopharyngeal carcinoma.

Keywords Autophagic flux · Carcinoma · Chemoresistance · HAX-1 · IGF2BP1 · Nasopharyngeal · Rab7a

Abbreviations

ABCC1	ATP-binding cassette transporter
ATG5	Autophagy related 5
CHX	Cycloheximide
Co-IP	Co-Immunoprecipitation
CQ	Chloroquine
DAPI	4′,6-Diamidino-2-phenylindole
DDP	Cisplatin
DEGs	Differentially expressed genes
EBSS	Earle Balanced Salt Solution
GAPDH	Glyceraldehyde-3-phosphate dehydrogenase
GEO	Gene Expression Omnibus
HAX-1	HS1-related protein X-1
HCQ	Hydroxychloroquine

✉ Wenjie Zheng
wenjiezheng@ntu.edu.cn

✉ Yiwen You
youyiwen_ent@163.com; youyiwen_nantong@163.com

✉ Bo You
youbo@ntu.edu.cn

[1] Department of Otorhinolaryngology Head and Neck Surgery, Affiliated Hospital of Nantong University, Xisi Road 20, Nantong 226019, Jiangsu Province, China

[2] Institute of Otolaryngology Head and Neck Surgery, Affiliated Hospital of Nantong University, Xisi Road 20, Nantong 226019, Jiangsu Province, China

[3] Fraunhofer Institute for Translational Medicine and Pharmacology (ITMP), Hamburg, Germany

[4] Fraunhofer Cluster of Excellence for Immune-Mediated Diseases (CIMD), Hamburg, Germany

[5] Department of General, Visceral and Cancer Surgery, Faculty of Medicine and University Hospital Cologne, University of Cologne, Cologne, Germany

[6] Research Center of Clinical Medicine, Nantong University Medical School, Affiliated Hospital of Nantong University, Nantong 226019, Jiangsu Province, China

[7] Department of Plastic and Reconstructive Surgery, Second Affiliated Hospital of Zhejiang University School of Medicine, Jiefang Road 88, Hangzhou, Zhejiang, P. R. China

Published online: 07 March 2025

IF	Immunofluorescence
IGF2BP1	Insulin-like growth factor 2 mRNA-binding protein 1
IHC	Immunohistochemistry
IP	Immunoprecipitation
KEGG	Kyoto Encyclopedia of Genes and Genomes
m6A	N^6-Methyladenosine
mIHC	Multiplex immunohistochemical
mRNA	Messenger RNA
NPC	Nasopharyngeal carcinoma
OS	Overall survival
P-gp	P-glycoprotein
qRT-PCR	Quantitative real-time PCR
shRNA	Small hairpin RNA
siRNA	Small interfering RNA
SNAP29	Synaptosome-associated protein 29
SNAREs	Soluble i-ethylmaleimide-sensitive factor attachment protein receptors
SQSTM1	Sequestosome 1
STX17	Syntaxin 17
TCGA	The Cancer Genome Atlas
VAMP8	Vesicle-associated membrane protein 8
WB	Western blot

Introduction

Cisplatin is considered one of the most potent and frequently prescribed anti-tumor chemotherapeutic agents, significantly improving survival rates in various solid tumors [1], including nasopharyngeal carcinoma (NPC). However, the development of resistance to cisplatin can diminish the drug's effectiveness, leading to cancer progression and potentially restricting future therapeutic options. This resistance may require the exploration of alternative treatments, which may not be as effective in managing the cancer, ultimately impacting the patient's prognosis and survival outcomes. According to the guidelines of the National Comprehensive Cancer Network (NCCN), the main curative treatment strategy for nasopharyngeal carcinoma (NPC) is intensity-modulated radiation therapy combined with cisplatin (DPP)-based chemotherapy [2, 3]. However, approximately 30 % of patients with NPC develop chemotherapeutic resistance, resulting in therapeutic failure and low survival [4–6]. Recent studies aimed at overcoming cisplatin resistance in tumors have focused on several innovative strategies. Researchers are investigating the use of combination therapies that incorporate novel agents, such as immune checkpoint inhibitors [7] and molecular targeted therapies [8]. Additionally, some experts have developed and examined survivin promoter-regulating conditionally replicating adenoviruses (CRAd) for their anti-tumor potential [1, 9], both alone and in combination with cisplatin, which can sensitize resistant tumor cells to this chemotherapeutic agent. These studies are groundbreaking and offer new insights into addressing cisplatin resistance. However, the role of autophagy in cisplatin resistance remains critical and must not be overlooked. Research within the past decade has established that autophagy plays a complex role in chemoresistance depending on the cancer type and treatment regimen; it can enhance cancer cell survival, thereby promoting chemoresistance, and promote apoptosis, thereby enhancing chemosensitivity [10]. For instance, autophagy has been shown to contribute towards *Fusobacterium nucleatum*-mediated colorectal cancer chemoresistance [11], whereas impaired lncRNA ARHGAP5-AS1 autophagic degradation promotes chemoresistance in chemoresistant gastric cancer cells [12]. Autophagy is a dynamic process comprising four critical steps, namely, initiation, nucleation/elongation/maturation, fusion to lysosomes, and degradation, thereby making its role in chemoresistance relatively complicated [13, 14]. Fusion of autophagosomes with lysosomes is an essential step in autophagic cargo degradation requiring activity of Rab GTPases, membrane-tethering complexes (HOPS complex and VPS genes), and soluble N-ethylmaleimide-sensitive factor attachment protein receptors (SNAREs) [15]. Additional autophagy relevant factors include inhibition of AXL kinase which decreases cytoprotective autophagic flux and induces immunogenic cell death in drug-resistant NSCLC cells [16]. Moreover, chloroquine and hydroxychloroquine can inhibit cytoprotective autophagy by interfering with autophagic flux, thereby promoting the sensitization of cancer cells to chemotherapy [17]. These studies have revealed the role of autophagic flux in chemoresistance and significant efforts are required to further characterize the role of autophagic flux in chemoresistance, and to identify autophagic vulnerability to overcome chemoresistance.

HS1-related protein X-1 (HAX-1) is a multifunctional protein cytogenetically located on chromosome 1q21 [18]. HAX-1 interacts with some cellular proteins, as well as mRNA 3′-UTR [18, 19], thereby contributing to the execution of multiple cellular processes, including anti-apoptotic processes, mitochondrial membrane potential-related processes, calcium signaling, actin remodeling, and mRNA surveillance [18–20]. We previously showed that HAX-1 promotes NPC angiogenesis by enhancing the translation efficiency of ITGB6 and activating the FAK pathway [21]. Furthermore, we showed that HAX-1 influences prognosis in patients with NPC and inhibits cancer cell death [22], suggesting that it may be involved in the development of chemoresistance. In the study reported herein, we investigated how HAX-1 affects DDP chemoresistance in patients with NPC and evaluated the underlying mechanism, and determined the relationship between HAX-1, IGF2BP1, and SQSTM1 expression and patient outcomes and DDP chemoresistance. Therefore, We hypothesized that

cisplatin chemoresistance based on the co-analysis of HAX-1, IGF2BP1, and SQSTM1 expression. Our findings may assist clinicians in identifying patients with low and high expression levels of HAX-1, IGF2BP1, and SQSTM1, enabling the treatment of those at high risk of chemoresistance with cisplatin-based chemotherapy. This approach could facilitate the selection of more tailored individual therapies.

Results

HAX-1 knockdown enhances NPC chemosensitivity to cisplatin

HAX-1 downregulation in CNE-2 cells via lentiviral infection and its overexpression significantly decreased and increased DDP IC_{50}, respectively (Fig. S1A–E). In addition, HAX-1 downregulation and DDP have significantly synergistic cytotoxicity (Fig. 1A–D, Fig. S1F–H). Furthermore, results of mouse tumor xenograft models confirmed that mice injected with low HAX-1-expressing cells (shHAX-1) exhibited reduced tumor growth and synergistic cytotoxicity of DDP exposure (Fig. 1E, F). Xenografts with low HAX-1 expression exhibited decreased ATP-binding cassette transporter (ABCC1) (chemoresistance marker, Fig. 1G), P-glycoprotein (P-gp, chemoresistance marker; Fig. 1G, H, J), and Ki-67 (marker of proliferation, Fig. 1H, I) levels. Analysis of SQSTM1 expression showed increased autophagic activity in low HAX-1-expressing xenografts (Fig. 1G, H, K). Furthermore, clinical data from The Cancer Genome Atlas (TCGA) cohort showed that patients with head and neck squamous cell carcinoma with high HAX-1 expression exhibited significantly shorter overall survival than those with low HAX-1 expression (Fig. 1L). We therefore suggest that levels of HAX-1 in NPC cells are inversely associated with sensitivity to cisplatin.

HAX-1 inhibited late stage autophagic flux in NPC cells

In order to study of the molecular mechanisms involved in HAX-1-mediated chemoresistance, we successfully established HAX-1 knockout cell lines using the CRISPR-Cas 9 gene editing approach (Fig. S2A, B). The results of RNA-seq analysis revealed 1,377 differentially expressed genes (DEGs) (adjusted p-value < 0.05, fold change >2.0; Fig. S2C). The Kyoto Encyclopedia of Genes and Genomes (KEGG) analysis was performed to identify HAX-1-related functional pathways with autophagy selected due its potential role in promoting chemoresistance (Fig. 2A). Thus, we evaluated the effects of HAX-1 on autophagosome and autolysosome generation. Interestingly, silencing HAX-1 resulted in decreased expression of LC3B-II and the autophagy substrate SQSTM1, whereas the LC3B-II:LC3B-I ratio, Beclin1 and ATG5 levels remained unchanged (Fig. 2B). We also showed that other autophagy receptors, such as NBR1, TAX1BP1 and OPTN in low HAX-1-expressing cells, have no significant change when compared to normal cells (Fig. 2B). This is consistent with a previous finding that the LC3-I to LC3-II conversion occurs during autophagosome elongation with LC3-II remaining membrane bound and degraded with the cargo. Additionally, SQSTM1, which is the best-known substrate of autophagy accumulates in autophagy deficiency status and our data suggest that HAX-1 may regulate its autophagic flux. Consistently, Immunofluorescence analysis of endogenous LC3 aggregation (Fig. 2C, D) and tandem monomeric mRFP-GFP-tagged LC3 analysis revealed that the number of autolysosomes increased significantly following HAX-1 knockdown; however, this effect was reversed following treatment with chloroquine (Fig. 2E, F). Using morphometric transmission electron microscopy, we observed an increase in autolysosome but not autophagosome counts, in response to HAX-1 knockdown (Fig. 2G). Moreover, HAX-1 expression positively correlated with SQSTM1 expression in head and neck squamous cell carcinoma tissues (Fig. 2H). Collectively, these results indicate that HAX-1 effectively inhibits late stage autophagic flux by blocking the fusion of autophagosomes with lysosomes.

SQSTM1/p62 is essential for HAX-1 mediated chemoresistance

SQSTM1/p62, an autophagy cargo adaptor protein, is mainly degraded by autophagy. We previously showed that silencing of HAX-1 results in SQSTM1 downregulation, indicating the blockage of autophagic flux. Here, we further investigated whether SQSTM1 reverses HAX-1 silencing-induced chemosensitivity. We successfully established a chemoresistant cell lines using CNE-2 cells (CNE-2R) and as expected, HAX-1, P-gp, and SQSTM1 expression was significantly increased in DDP-resistant CNE-2R cells (Fig. S2D). In addition, ABCC1, P-gP, and SQSTM1 expression significantly decreased upon HAX-1 knockdown (Fig. S2E–G); however, this was significantly reversed upon the induction of SQSTM1 overexpression (Fig. S2E–G). Moreover, mouse tumor xenograft experiments showed that HAX-1 knockdown could significantly decrease tumor growth, as well as Ki-67, SQSTM1, and P-gp expression; however, this effect was reversed following the induction of SQSTM1 overexpression (Fig. S2H–L). Next, we performed rescue experiments to measure chemosensitivity. These cellular assays revealed that SQSTM1 overexpression inhibited HAX-1 knockdown-induced decrease in cell proliferation (Fig. S3A–E). These results demonstrated that the DDP chemoresistance-promoting effect of HAX-1 is dependent

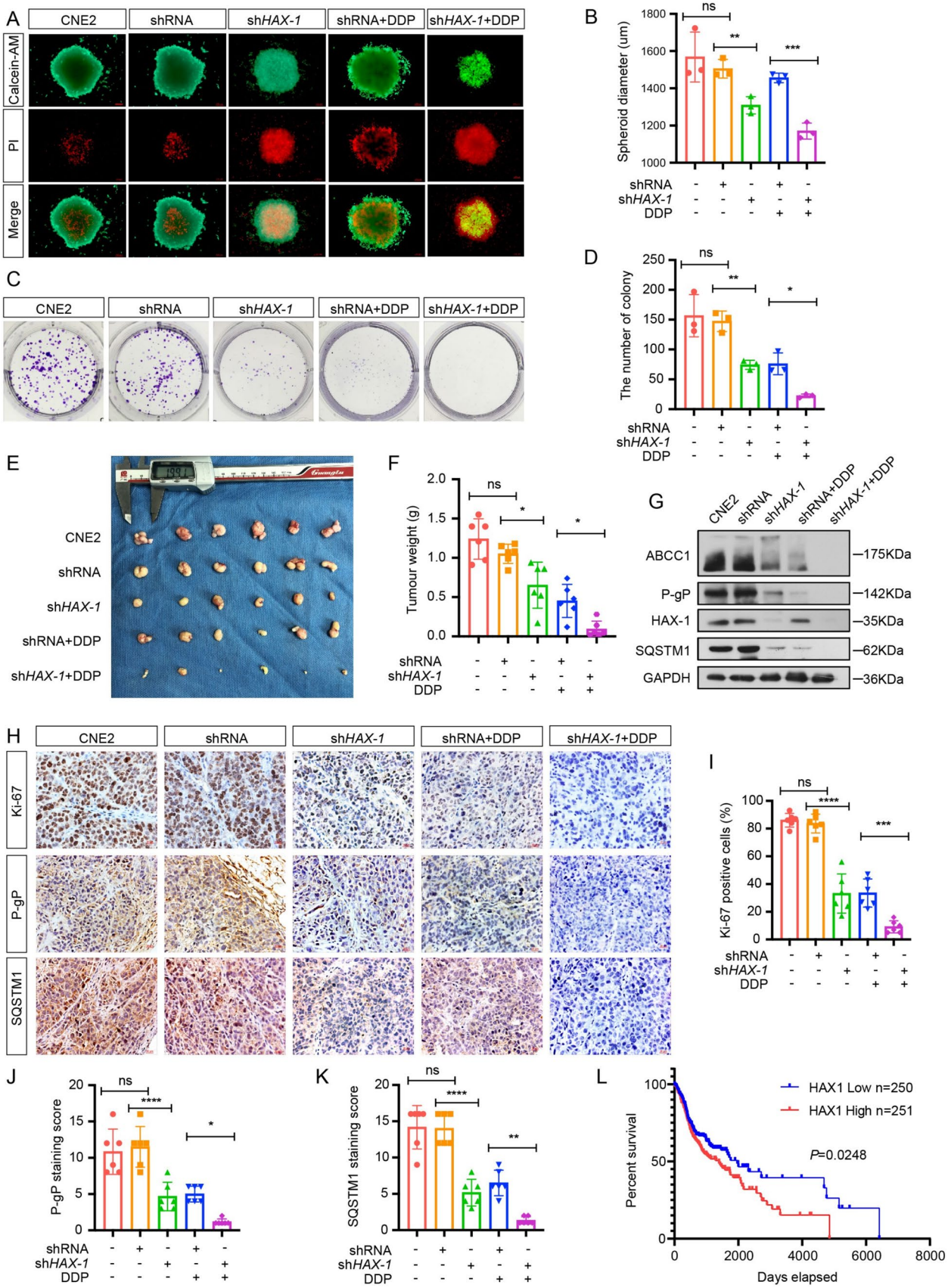
A
CNE2
shRNA
shHAX-1
shRNA+DDP
shHAX-1+DDP
Calcein-AM
PI
Merge
B
Spheroid diameter (um)
ns
**
***
shRNA
shHAX-1
DDP
C
CNE2
shRNA
shHAX-1
shRNA+DDP
shHAX-1+DDP
D
The number of colony
ns
**
*
E
CNE2
shRNA
shHAX-1
shRNA+DDP
shHAX-1+DDP
F
Tumour weight (g)
ns
*
*
G
CNE2
shRNA
shHAX-1
shRNA+DDP
shHAX-1+DDP
ABCC1
P-gP
HAX-1
SQSTM1
GAPDH
175KDa
142KDa
35KDa
62KDa
36KDa
H
Ki-67
P-gP
SQSTM1
I
Ki-67 positive cells (%)
ns
****
***
J
P-gP staining score
ns
****
*
K
SQSTM1 staining score
ns
****
**
L
HAX1 Low n=250
HAX1 High n=251
P=0.0248
Percent survival
Days elapsed

◂**Figure 1** HAX-1 association with NPC chemoresistance and patient outcomes. **A**, **B** Three-dimensional spheroid formation and **C**, **D** colony formation analyses for cell proliferation after transfection with HAX-1-specific shRNA or control shRNA, with or without DDP exposure (one-way ANOVA). **E** shRNA or shHAX-1 transfected CNE2 cells were inoculated into BALB/c nude mice. DPP or an equivalent volume of PBS was administered at a dosage of 4 mg/kg body weight every two days, commencing when the tumor sizes reached 0.125 cm^3. After 28 days, the tumors were harvested for measurement of their sizes and weights. The data are presented as individual dots representing the weight of each tumor, with the scale bars indicating the mean±standard error of the mean (SEM) of tumor weights from six mice in each treatment group of the representative experiment (mean±SEM, n = 6). Statistical analysis was conducted using a two-tailed unpaired t-test. **F** Statistical analysis of tumor weight on day 28. **G** Tumor WB analysis and **H–K** IHC staining for ABCC1, P-gP, HAX-1, Ki-67, and SQSTM1 expression (one-way ANOVA). **L** Kaplan-Meier analysis comparing overall survival in the TCGA database using the Log-rank test. All data are presented as the mean ± SEM of at least three independent experiments. *$P < 0.05$, ** $P < 0.01$, *** $P < 0.001$, **** $P < 0.0001$. *WB* western blot, *PI* dead cells, *Calcein-AM* live cells; Scale bar: 200 μm

on its ability to inhibit late stage autophagic flux, which requires SQSTM1 accumulation.

HAX-1 overexpression blocks autophagic flux by competitively binding to Rab7a

In order to further investigate the mechanism underlying HAX-1 mediated autophagic flux blockade, we identified 493 HAX-1 interacting molecules involved in autophagic flux by Co-IP and mass spectrometry. Amongst these proteins, the Ras-associated protein, RAB7A (Rab7a), is considered to be the key component that regulates autophagosome-lysosome fusion [23], and therefore of further interest (Fig. 3A). This was confirmed by co-precipitation of endogenous HAX-1 and Rab7a and in the reverse configuration, namely endogenous Rab7a and HAX-1, respectively (Fig. 3B). As a consequence, HAX-1 and Rab7a proteins largely colocalized as expected (Fig. 3C). In order to determine the interaction domains between HAX-1 and Rab7a, Co-IP analyses were carried out using four truncated HAX-1 mutants. The deletion mutant, HA-HAX-1 1−128, was shown to be strongly bound to Rab7a but not with any other deletion mutant (Fig. 3D), suggesting that HAX-1 directly binds to Rab7a via its domain at the 100–128 amino acid sequence.

Rab7a is considered to be the main mediator of membrane tethering and determines the site of fusion. However, the fusion of autophagosomes with lysosomes depends on tethering complexes and small transmembrane proteins (SNAREs) [24, 25]. During autophagosome-lysosome fusion, Rab7a binds to the hexameric HOPS tethering complex; this is followed by SNARE-mediated fusion through binding to SNAREs and promoting their assembly [24]. Consequently, we hypothesized that HAX-1 competitively binds to Rab7a, reducing its interaction with SNAREs and blocking autophagosome-lysosome fusion. Interestingly, as compared to the control group, in the HAX-1 overexpression group, the combination and colocalization of Rab7a and the SNARE complex, consisting of syntaxin 17 (STX17), synaptosome-associated protein 29 (SNAP29), and vesicle-associated membrane protein 8 (VAMP8), significantly decreased; however, binding of Rab7a with SNAREs increased with HAX-1 downregulation (Fig. 3E, F), further strengthening the hypothesis that HAX-1 competitively binds to Rab7a, thereby reducing its interaction SNAREs and blocking autophagic flux.

HAX-1 recruits ubiquitin E3 ligase (NEDD4) to regulate Rab7a protein stability

HAX-1 contains a PEST domain, a rapid regulator of protein degradation, at its 104–117 amino acid sequence [18, 26]. Based on Co-IP findings (Fig. 3D), we hypothesized that HAX-1 regulates Rab7a stability by binding to its PEST domain. First, we found that HAX-1 did not affect Rab7a mRNA levels (Fig. 4A). Next, using a proteasome inhibitor (MG-132) and several autophagy inhibitors (3MA, chloroquine, and Bafa1), we assessed whether the post-translational pathway was relevant for Rab7a stability. We found that only MG132 significantly increased Rab7a protein expression (Fig. 4B). Moreover, Rab7a levels were significantly downregulated and upregulated following the induction and downregulation of HAX-1 overexpression, respectively (Fig. 4C). These results indicated that HAX-1 participated in ubiquitin-proteasome pathway (UPP)-mediated Rab7a degradation. Subsequently, Rab7a downregulation and subsequent ubiquitination analyses showed that inhibiting HAX-1 activity significantly suppressed Rab7a ubiquitination, while HAX-1 overexpression enhanced its ubiquitination (Fig. 4C). The UbiBrowser database was used to identify the E3 ubiquitin ligase that participates in Rab7a ubiquitination and of the four main E3 ubiquitin ligases that participate in Rab7a ubiquitination, only NEDD4 was commonly identified (Fig. 4D and Fig. S4A). Additionally, Co-IP showed an interaction between Rab7a and NEDD4 (Fig. 4E) and this significantly increased with HAX-1 overexpression and decreased with HAX-1 knockdown (Fig. 4F), further confirming that HAX-1 was necessary for the binding of NEDD4 with Rab7a. To further verify whether NEDD4 is critical for Rab7a degradation, NEDD4 knockdown using three lentiviral vectors (shRNA, shNEDD4-1, and shNEDD4-3) resulted in the highest knockdown efficiency (Fig. 4G). As expected, NEDD4 knockdown using shNEDD4-1 and shNEDD4-3 induced a significant increase in Rab7a levels (Fig. 4G). In addition, rescue experiments showed that NEDD4 knockdown reversed HAX-1 overexpression-induced Rab7a expression inhibition (Fig. 4H),

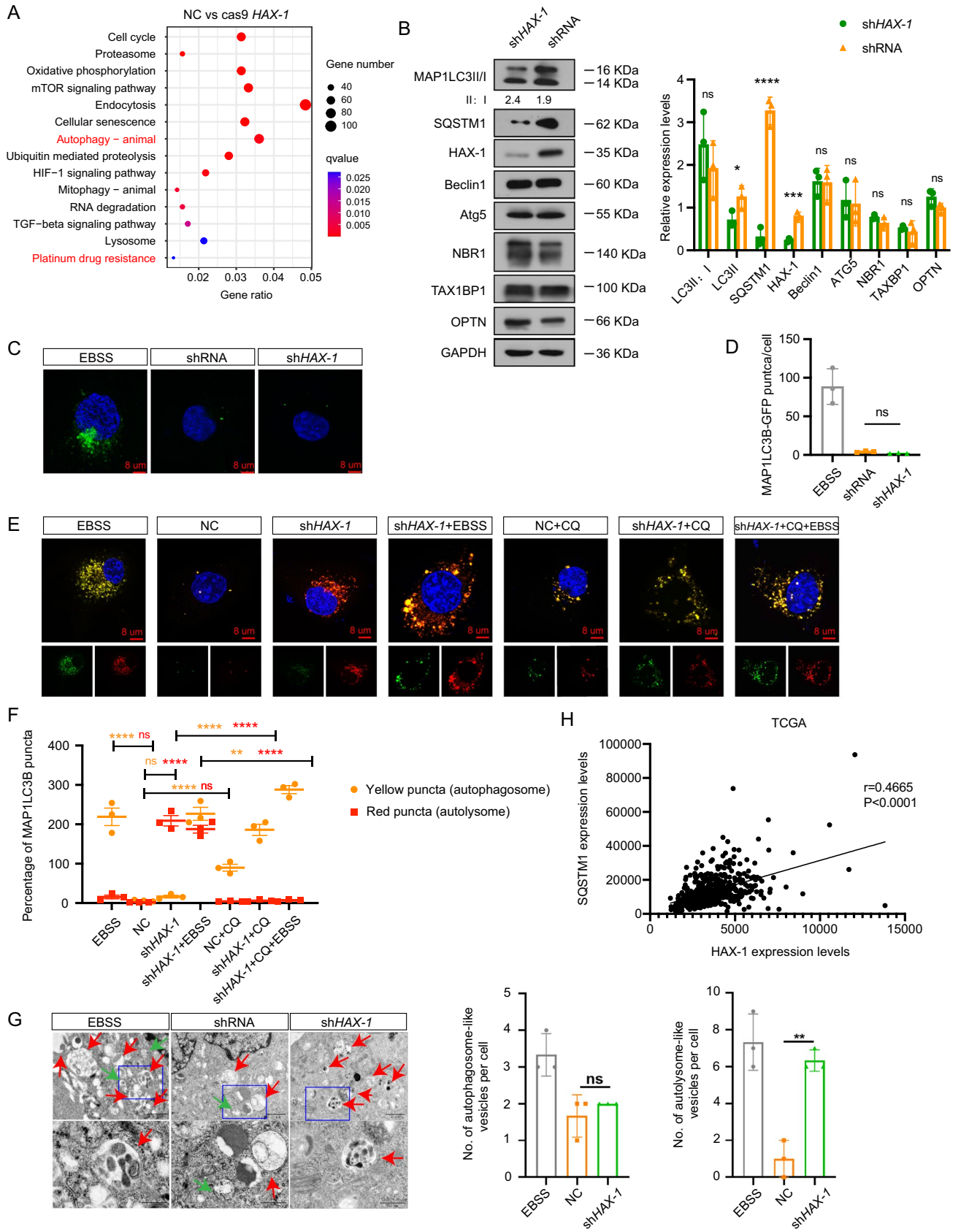
A
NC vs cas9 HAX-1
Cell cycle
Proteasome
Oxidative phosphorylation
mTOR signaling pathway
Endocytosis
Cellular senescence
Autophagy − animal
Ubiquitin mediated proteolysis
HIF−1 signaling pathway
Mitophagy − animal
RNA degradation
TGF−beta signaling pathway
Lysosome
Platinum drug resistance
0.02 0.03 0.04 0.05
Gene ratio
Gene number
40
60
80
100
qvalue
0.025
0.020
0.015
0.010
0.005
B
shHAX-1
shRNA
MAP1LC3II/I
16 KDa
14 KDa
II: I
2.4 1.9
SQSTM1
62 KDa
HAX-1
35 KDa
Beclin1
60 KDa
Atg5
55 KDa
NBR1
140 KDa
TAX1BP1
100 KDa
OPTN
66 KDa
GAPDH
36 KDa
shHAX-1
shRNA
Relative expression levels
LC3II: I
LC3II
SQSTM1
HAX-1
Beclin1
ATG5
NBR1
TAXBP1
OPTN
C
EBSS
shRNA
shHAX-1
8 um
D
MAP1LC3B-GFP puntca/cell
EBSS
shRNA
shHAX-1
E
EBSS
NC
shHAX-1
shHAX-1+EBSS
NC+CQ
shHAX-1+CQ
shHAX-1+CQ+EBSS
8 um
F
Percentage of MAP1LC3B puncta
Yellow puncta (autophagosome)
Red puncta (autolysome)
EBSS
NC
shHAX-1
shHAX-1+EBSS
NC+CQ
shHAX-1+CQ
shHAX-1+CQ+EBSS
H
TCGA
SQSTM1 expression levels
HAX-1 expression levels
r=0.4665
P<0.0001
G
EBSS
shRNA
shHAX-1
No. of autophagosome-like vesicles per cell
No. of autolysome-like vesicles per cell
EBSS
NC
shHAX-1

◂**Figure 2** HAX-1 induced blockade of late-stage autophagic flux in NPC cells. **A** DEGs between HAX-1 knockout and control cell lines clustered using KEGG pathway terms. **B** WB analysis of autophagic flux-related protein levels. Student's *t*-tests. **C**, **D** IF analysis of endogenous LC3 puncta (one-way ANOVA). **E**, **F** mRFP-GFP-LC3 reporters transfected into CNE-2 for the detection of autophagic flux (two-way ANOVA). **G** TEM analysis of endogenic autophagic microstructure (red and green arrowheads represent cellular autolysosome-like and autophagosome-like vesicles, respectively). **H** Pearson correlation between HAX-1 and SQSTM1 expression in TCGA database (linear regression). All data are presented as the mean ± SEM of at least three independent experiments. *$P < 0.05$, **$P < 0.01$, ****$P < 0.0001$. *DEGs* differentially expressed genes, *WB* western blot, *IF* immunofluorescence, *CQ* chloroquine, *EBSS* Earle balanced salt solution

improved its ubiquitination capacity (Fig. 4I), and shortened its half-life following treatment with CHX to block protein translation (Fig. 4J). These results indicated that HAX-1 serves as a scaffold for NEDD4 recruitment, thereby promoting Rab7a degradation.

Next, we evaluated the involvement of Rab7a in HAX-1-mediated chemosensitivity. Rab7a downregulation significantly abrogated HAX-1 knockdown-mediated suppression of SQSTM1 (Fig. S4B, C), and inhibited cell proliferation *in-vitro* (Fig. S4D–J) and *in-vivo* (Fig. S4K) as well as decreased the HAX-1 knockdown-mediated SQSTM1 and P-gp expression levels in xenografts (Fig. S4L). Collectively, our data demonstrated that HAX-1 not only accelerated Rab7a degradation, but also inhibited the binding of Rab7a with SNAREs by binding to Rab7a, thereby blocking autophagic flux.

HAX-1 regulates mRNA stability and IGF2BP1 translation

HAX-1 not only interacts with certain proteins, but also binds to mRNA 3′-UTRs [18, 19]. Addition of N-6-methyladenosine (m6A), the most common mRNA modification in eukaryotes, is mediated by methyltransferase complexes ("writers"), demethylases ("erasers"), and RNA-binding proteins ("readers") [27]. Dysregulated m6A modifier levels can mediate chemoresistance [28, 29]. Thus, we investigated the role of a dysregulated m6A machinery in the upregulation of HAX-1-mediated DDP chemoresistance. We re-analyzed our RNA-seq data in Fig. S2C and found that m6A modifiers were significantly downregulated in HAX-1 knockout cells (Fig. 5A). However, only the levels of IGF2BP1 protein (Fig. 5B) and mRNA (Fig. 5C) were significantly decreased and increased, respectively, following the downregulation and upregulation of HAX-1 (Fig. 5B, C). Furthermore, there was no significant difference in promoter activity (Fig. 5D), suggesting that HAX-1 did not affect IGF2BP1 transcription. HAX-1 overexpression or knockdown had no significant effect on the half-life of IGF2BP1 precursor mRNA (Fig. 5E). However, HAX-1 plays an essential role in delaying mature IGF2BP1 mRNA degradation (Fig. 5F). We further investigated the potential mechanisms involved in HAX-1-mediated regulation of IGF2BP1 expression. Our data showed that MG-132 attenuated HAX-1-mediated IGF2BP1 expression; however, this was not the case with CHX (Fig. 5G, H), suggesting that HAX-1 may regulate IGF2BP1 mRNA stability and translation. This was confirmed by the observation that the half-life of IGF2BP1 was not significantly different between cells with different HAX-1 expression levels (Fig. 5I).

IGF2BP1 stabilizes HAX-1 mRNA in an m6A-dependent manner

IGF2BP1 can recognize and bind to m6A sites on mRNA and plays a role in stabilizing mRNA and promoting its translation. As HAX-1 mRNAs have several m6A sites in their CDS regions (Fig. 6A), we investigated whether IGF2BP1 could regulate HAX-1 expression in an m6A-dependent manner. We found that IGF2BP1 downregulated HAX-1 mRNA expression (Fig. 6B); silencing IGF2BP1 suppressed the binding of IGF2BP1 with HAX-1 mRNA (Fig. 6C) and downregulated HAX-1 mRNA m6A levels (Fig. 6D). Notably, IGF2BP1 downregulation significantly decreased HAX-1 mRNA and protein expression (Fig. 6E–G). HAX-1 overexpression partially reversed the decrease in P-gp and SQSTM1 expression levels induced by IGF2BP1 silencing (Fig. 6F). In addition, silencing HAX-1 promoted IGF2BP1 knockdown-induced inhibition of P-gp and SQSTM1 expression (Fig. 6G). Moreover, IGF2BP1 did not affect HAX-1 promoter activity (Fig. 6H) nor the half-life of HAX-1 precursor mRNA (Fig. 6I); however, it significantly enhanced the stability of mature HAX-1 mRNA (Fig. 6J). Furthermore, MG-132, but not CHX, attenuated IGF2BP1-mediated HAX-1 expression (Fig. 6K, L). Collectively, these findings imply that IGF2BP1 binds to HAX-1 mRNA harboring m6A modifications and regulates its stability.

The IGF2BP1/HAX-1/ Rab7a axis is essential for chemoresistance

We further assessed whether the IGF2BP1-HAX-1 positive feedback loop was essential for Rab7a-mediated chemosensitivity. Rab7a upregulation or downregulation significantly abrogated the IGF2BP1 knockdown-mediated suppression of cell proliferation *in-vitro* (Fig. S5A–F) and *in-vivo* (Fig. S5G), as well as the HAX-1 knockdown-mediated decrease in SQSTM1 and P-gp expression (Fig. S5H, I). Moreover, compared to IGF2BP1 and Rab7a silencing, HAX-1 upregulation as well as IGF2BP1 and Rab7a silencing significantly promoted cell proliferation and SQSTM1

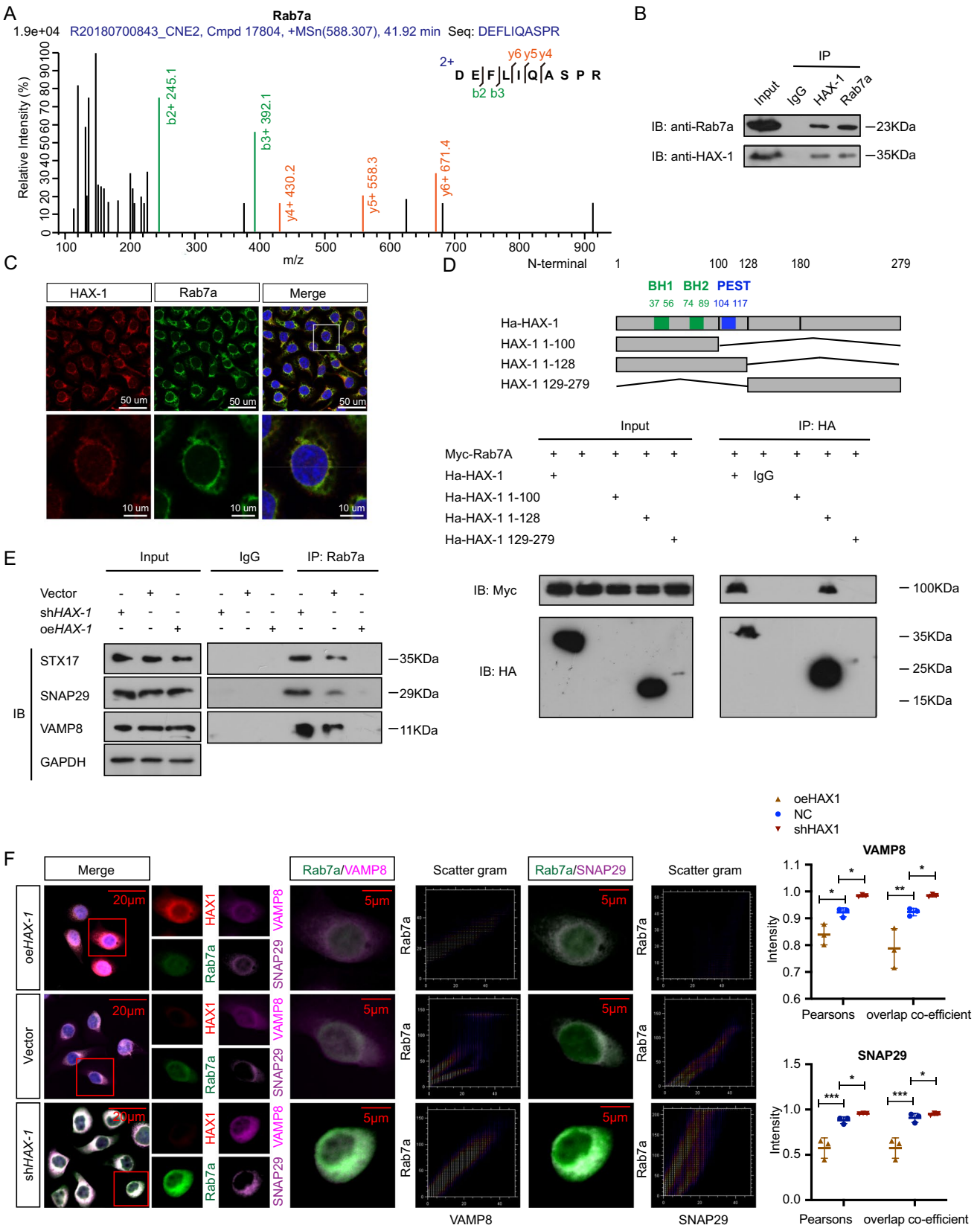
A
Rab7a
1.9e+04 R20180700843_CNE2, Cmpd 17804, +MSn(588.307), 41.92 min Seq: DEFLIQASPR
Relative Intensity (%)
m/z
b2+ 245.1
b3+ 392.1
y4+ 430.2
y5+ 558.3
y6+ 671.4
2+
y6 y5 y4
D E F L I Q A S P R
b2 b3
B
IP
Input
IgG
HAX-1
Rab7a
IB: anti-Rab7a
IB: anti-HAX-1
23KDa
35KDa
C
HAX-1
Rab7a
Merge
50 um
10 um
D
N-terminal
1
100
128
180
279
BH1 BH2 PEST
37 56 74 89 104 117
Ha-HAX-1
HAX-1 1-100
HAX-1 1-128
HAX-1 129-279
Input
IP: HA
Myc-Rab7A
Ha-HAX-1
IgG
Ha-HAX-1 1-100
Ha-HAX-1 1-128
Ha-HAX-1 129-279
IB: Myc
IB: HA
100KDa
35KDa
25KDa
15KDa
E
Input
IgG
IP: Rab7a
Vector
shHAX-1
oeHAX-1
IB
STX17
SNAP29
VAMP8
GAPDH
35KDa
29KDa
11KDa
F
oeHAX1
NC
shHAX1
Merge
Rab7a/VAMP8
Scatter gram
Rab7a/SNAP29
Scatter gram
oeHAX-1
Vector
shHAX-1
20μm
5μm
HAX1
Rab7a
VAMP8
SNAP29
VAMP8
SNAP29
Intensity
Pearsons
overlap co-efficient

◂**Figure 3** HAX-1 mediated blockade of autophagic flux via interaction with Rab7a. **A** Demonstration of Rab7a interaction with HAX-1-interacting protein by Co-IP and mass spectrometric analyses. **B** Detection of interaction between exogenous HAX-1 and Rab7a by Co-IP. **C** Colocalization of HAX-1 and Rab7a confirmed through IF staining. **D** Requirement of amino acid sequence spanning HAX-1 1–128 for interaction with Rab7a. **E** Effects of HAX-1 on the binding of Rab7a with the SNARE complex identified through Co-IP. **F** Representative IF images (left) and statistical diagrams (right) showing effects of HAX-1 on the colocalization of Rab7a and the SNARE complex (one-way ANOVA). All data are presented as the mean ± SEM of at least three independent experiments. $*P < 0.05$, $**P < 0.01$, $***P < 0.001$. Co-IP co-immunoprecipitation

and P-gp expression (Fig. S5A–F), highlighting the involvement of the IGF2BP1-HAX-1 positive feedback loop in Rab7a-mediated chemosensitivity.

HAX-1, IGF2BP1, and autophagy substrate (SQSTM1) levels correlate and are clinically relevant in NPC patients

Multiplex IHC (mIHC) assays were performed to investigate the clinical significance of HAX-1, IGF2BP1, and SQSTM1 in NPC. As shown in Fig. 7A, HAX-1, IGF2BP1, and SQSTM1 were highly expressed in the tumor tissues of chemoresistant NPC patients, but not in those of chemosensitive patients and were absent in normal tissues (Fig. 7A). Furthermore, IHC with NPC tissue microarrays showed that HAX-1, IGF2BP1, and SQSTM1 were significantly upregulated in NPC tissues as compared to normal tissues (Fig. S6A–L), with their levels being more prominent in patients with clinical stage IV cancer (Fig. 7B, C, Table S1), lymph node metastases (Fig. S6A–L, Table S1), recurrence (Fig. S6A–L, Table S1), and distant metastases (Fig. S6A–L, Table S1). HAX-1 expression in NPC tissues was positively correlated with IGF2BP1 and SQSTM1 levels; in addition, IGF2BP1 levels were positively correlated with SQSTM1 expression (Fig. 7D). Furthermore, Kaplan-Meier analyses showed that HAX-1, IGF2BP1, and SQSTM1 upregulation was significantly correlated with poor clinical outcomes (5-year overall survival (OS): 84.38 % VS 93.75 % for HAX-1; 5-year OS: 77.55 % vs 96.83 % for IGF2BP1; 5-year OS: 80.49 % vs 94.37 % for SQSTM1; Fig. 7E). Thus, we constructed a survival prediction model based on the co-analysis of HAX-1, IGF2BP1, and SQSTM1 expression. Patients were stratified into three risk groups: (1) the low-risk DDP chemoresistance group (low-level HAX-1, IGF2BP1, and SQSTM1 expression) comprising 35 patients (32.25 %), (2) the intermediate-risk DDP chemoresistance group (high expression levels of one or two of the markers, HAX-1, IGF2BP1, and SQSTM1) comprising 48 patients (42.86 %), and (3) the high-risk DDP chemoresistance group (high HAX-1, IGF2BP1, and SQSTM1 expression levels) comprising 29 patients (25.89 %). Our data demonstrated that when compared to patients in the other groups, those in the high-risk group had the worst overall survival (OS) (5-year OS: 68.97 %; Fig. 7F). This finding was confirmed using data from a cohort in TCGA database (Fig. 7G). These results indicate that the survival prediction model for NPC DDP chemoresistance based on the co-analysis of HAX-1, IGF2BP1, and SQSTM1 expression is an appropriate and valuable prognostic tool (Fig. 8).

Discussion

Consistent with previous studies, which suggested that HAX-1 promotes chemoresistance in breast cancer [30, 31], laryngeal cancer [32], and bladder cancer [33], this study showed that HAX-1 serves as a DPP resistance-promoting oncogene in NPC. In addition, this study described a novel mechanism of action for the involvement of HAX-1 in chemoresistance i.e., the inhibition of autophagic flux. Decreased autophagic activity induces tumor suppression in NPC [34–36] together with the dysregulation of critical autophagic genes [34–36]. However, the functional role of autophagic flux in NPC chemoresistance has not yet been elucidated. Our data, which is based on transcriptomic and mRFP-GFP-tagged LC3 analyses, show that HAX-1 effectively inhibits late stage autophagic flux. HAX-1 silencing blocked autophagosome and lysosome fusion, as well as downregulated the level of the autophagy cargo adaptor protein, SQSTM1. Studies on NPC have shown that SQSTM1 is significantly involved in chemosensitivity [37, 38], and this is consistent with our finding that SQSTM1 expression was significantly increased in DDP-resistant cells. Consistently, rescue experiments demonstrated that SQSTM1 reversed HAX-1 silencing-induced chemosensitivity. Our data provide new insights into the clinical applications of autophagic flux-related therapies that target DPP chemoresistance in NPC.

Here, we identified Rab7a as a novel interacting biomolecule of HAX-1. Although Rab7a has been extensively reported to regulate autophagosome-lysosome fusion, our work is the first study to report that HAX-1 blocks autophagic flux by directly binding to Rab7a. HAX-1 contains two putative Bcl-2 homology domains, BH1 and BH2, with low similarity, a PEST motif, and a C-terminal transmembrane domain, which is mainly responsible for its interactions with other proteins. Our data indicates that HAX-1 directly binds to Rab7a via its PEST domain. Moreover, we demonstrated that the HAX-1 PEST domain serves as a scaffold for recruiting NEDD4 which binds to Rab7a and degrades it. Previous studies have reported the PEST domain to be a rapid regulator of protein degradation [39, 40]. Our data shows that Rab7a directly binds to the HAX-1 PEST sequence and may inhibit the exposure of caspase cleavage

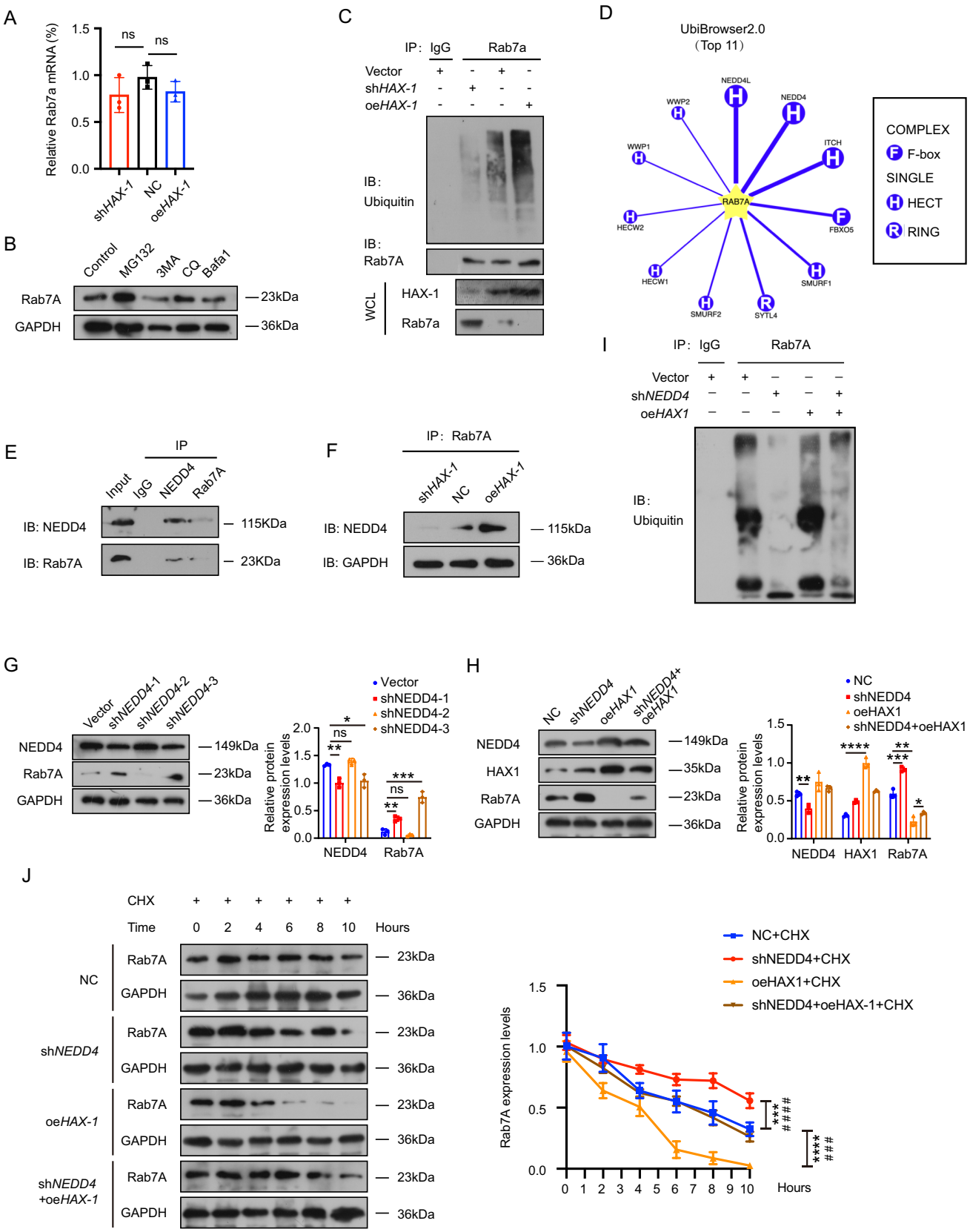
A
Relative Rab7a mRNA (%)
ns
ns
shHAX-1
NC
oeHAX-1
B
Control
MG132
3MA
CQ
Bafa1
Rab7A
GAPDH
23kDa
36kDa
C
IP: IgG
Rab7a
Vector
shHAX-1
oeHAX-1
IB: Ubiquitin
IB: Rab7A
WCL
HAX-1
Rab7a
D
UbiBrowser2.0
(Top 11)
NEDD4L
WWP2
NEDD4
WWP1
ITCH
RAB7A
HECW2
FBXO5
HECW1
SMURF1
SMURF2
SYTL4
COMPLEX
F-box
SINGLE
HECT
RING
E
IP
Input
IgG
NEDD4
Rab7A
IB: NEDD4
IB: Rab7A
115KDa
23KDa
F
IP: Rab7A
shHAX-1
NC
oeHAX-1
IB: NEDD4
IB: GAPDH
115kDa
36kDa
I
IP: IgG
Rab7A
Vector
shNEDD4
oeHAX1
IB: Ubiquitin
G
Vector
shNEDD4-1
shNEDD4-2
shNEDD4-3
NEDD4
Rab7A
GAPDH
149kDa
23kDa
36kDa
Relative protein expression levels
NEDD4
Rab7A
H
NC
shNEDD4
oeHAX1
shNEDD4+oeHAX1
HAX1
149kDa
35kDa
23kDa
36kDa
NEDD4
HAX1
Rab7A
J
CHX
Time
0 2 4 6 8 10 Hours
NC
shNEDD4
oeHAX-1
shNEDD4 +oeHAX-1
23kDa
36kDa
NC+CHX
shNEDD4+CHX
oeHAX1+CHX
shNEDD4+oeHAX-1+CHX
Rab7A expression levels
Hours

◂**Figure 4** HAX-1 accelerates Rab7a degradation via recruiting NEDD4. **A** Evaluation of the regulatory role of HAX-1 on Rab7a mRNA level using RT-PCR. **B** WB analysis of Rab7a levels (GAPDH was used as a control). **C** Ubiquitination of endogenous Rab7a as determined by Co-IP. **D** Prediction of E3 ubiquitin ligase-targeting Rab7a using the Ubibrowser database (ubibrowser.ncpsb.org/) with the top 11 E3 ubiquitin ligases displayed. **E** Interaction between Rab7a and NEDD4 as determined by Co-IP. **F** Regulatory role of HAX-1 on the interaction between Rab7a and NEDD4 as determined by Co-IP. **G** WB analysis of Rab7a and NEDD4 levels (GAPDH was used as the control). **H** WB analysis of NEDD4, HAX-1, and Rab7a levels (GAPDH used as control). **I** Rab7a ubiquitination as determined by IP. **J** Expression of Rab7a in CNE-2 cells treated with NEDD4-specific shRNA and/or target HAX-1-overexpressing lentiviruses in the presence of CHX for the indicated time points as determined by IP (two-way ANOVA). All data are presented as the mean ± SEM of at least three independent experiments. ***$P < 0.001$, ****$P < 0.0001$. *Co-IP* co-immunoprecipitation, *WB* western blot

sites, as well as HAX-1 proteasomal degradation. Rab7a is a member of the small GTPase family whose activation and inactivation is precisely controlled to regulate autophagosome transport and fusion [24, 41, 42]. Aside from the role of HAX-1 in promoting Rab7a degradation clarified in this study, it would be of significant research interest to further clarify how each Rab7a activation and inactivation cycle is regulated and whether HAX-1 drives Rab7a inactivation.

Recently, m6A RNA modification was reported to affects NPC progression; for example, METTL3-, METTL5-, VIRMA-, and WTAP-mediated m6A modifications are required for NPC tumorigenesis and metastasis [43–46]. Moreover, the specificity and critical roles of m6A methylation have been described for certain targets. It has been reported that m6A-modified CBX1, long non-coding RNA (FAM225A), and 18S rRNA promote NPC progression and immune evasion [44, 47, 48]. Furthermore, m6A is highly enriched in TRIM11, and TEAD4 enhances DPP resistance in NPC [38, 49]. IGF2BP1, a m6A reader, has traditionally been regarded as an oncogene and is a potential therapeutic target for cancers; however, little is known about its role in NPC. In our study, we identified HAX-1 as a novel m6A methylation target and found that IGF2BP1 recognizes HAX-1 m6A methylation and enhances its stability. In addition, we found that HAX-1 not only interacts with Rab7a, but also binds to IGF2BP1 mRNA, thereby contributing to IGF2BP1 mRNA stability and translation. To the best of our knowledge, our study is the first report that HAX-1 is a direct regulator of IGF2BP1 mRNA stability. Collectively, our data provide new insights into the function of the HAX-1/IGF2BP1 positive feedback loop in chemoresistance.

Appropriate treatment choices depend on accurate prognostic assessment. There is no effective forecasting model that accurately identifies patients with high DDP chemoresistance risk. In our study, we constructed a survival prediction model for NPC DDP chemoresistance based on the co-analysis of HAX-1, IGF2BP1, and SQSTM1 expression. This model can help clinicians to identify low HAX-1-, IGF2BP1-, and SQSTM1-expressing patients who can receive DPP-based chemotherapy and high HAX-1-, IGF2BP1-, and SQSTM1-expressing patients with a high chemoresistance risk; this may facilitate the selection of more appropriate individual therapies.

In summary, our study provides compelling evidence of the vital role played by HAX-1 in chemoresistance and characterizes the mechanism by which it blocks autophagic flux (Fig. 8). In addition, we identified Rab7a and IGF2BP1 mRNA as novel HAX-1-interacting biomolecules. Moreover, our findings suggest that the regulation of HAX-1 mRNA stability via m6A methylation could be a new direction for future research. Our data provide evidence of the usefulness of HAX-1, IGF2BP1, and SQSTM1 levels in predicting clinical outcomes and DDP chemoresistance risk. Our findings may facilitate future studies on DDP chemoresistance. Additionally, the current research predominantly examines cisplatin resistance. Future studies should include a broader range of chemotherapy agents to ascertain the generalizability of HAX-1, IGF2BP1, and SQSTM1, thereby expanding the scope of the research.

Materials and methods

Key resources table

Reagent or Resource	Source	Identifier
Antibodies		
HAX-1	ABclonal	A5551
ABCC1	ABclonal	A2223
P glycoprotein	proteintech	22336-1-AP
KI67	proteintech	27309-1-AP
SQSTM1	proteintech	18420-1-AP
Beclin 1	proteintech	11306-1-AP
ATG5	proteintech	10181-2-AP
LC3	proteintech	14600-1-AP
NBR1	proteintech	16004-1-AP
OPTN	proteintech	10837-1-AP
TAX1BP1	proteintech	14424-1-AP
Rab7a	proteintech	55469-1-AP
Lamp1	Santa Cruz Biotechnology	sc-20011
SNAP29	proteintech	12704-1-AP
VAMP8	proteintech	15546-1-AP
STX17	proteintech	17815-1-AP

Figure 5

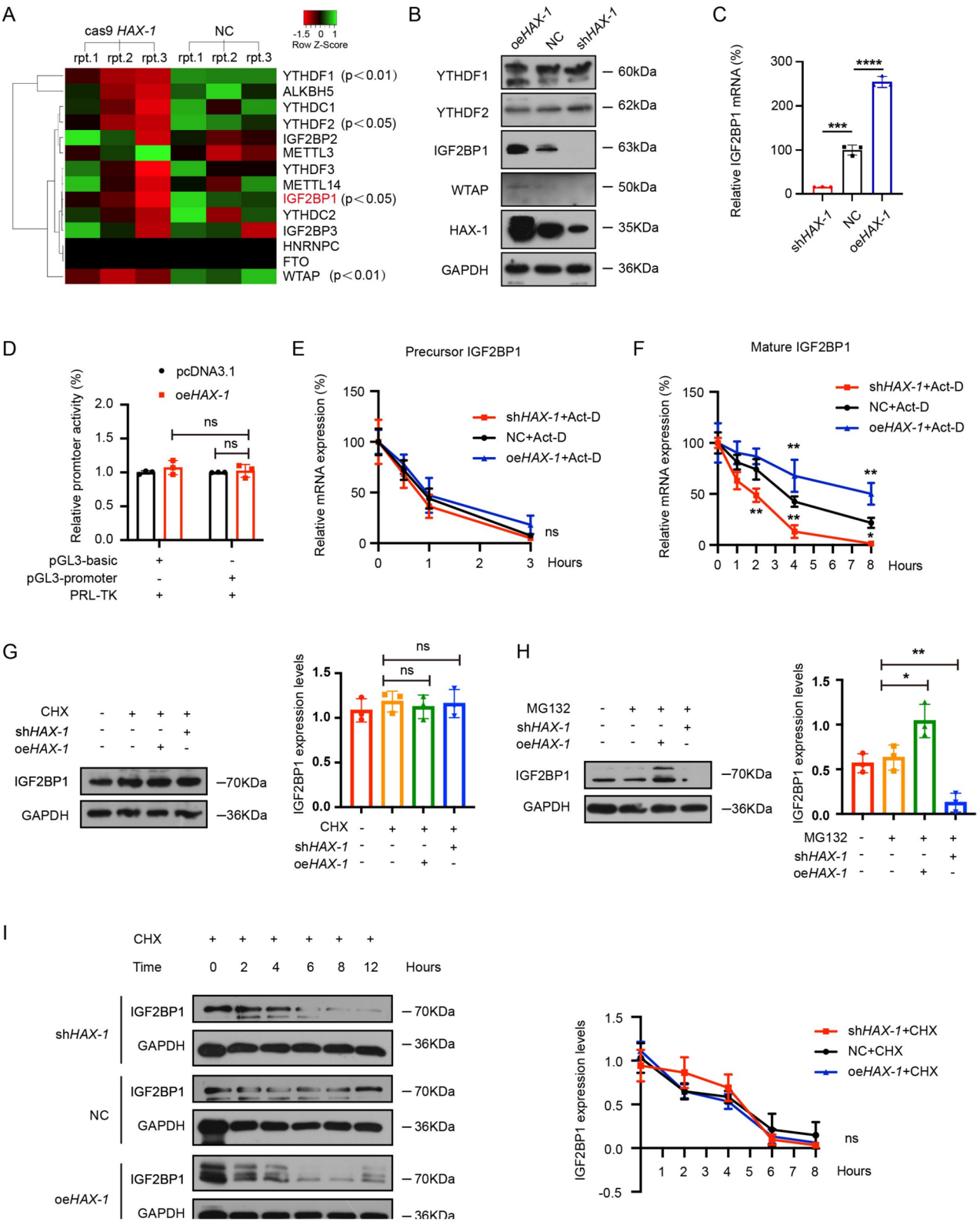
A
cas9 HAX-1
NC
rpt.1 rpt.2 rpt.3 rpt.1 rpt.2 rpt.3
-1.5 0 1
Row Z-Score
YTHDF1 (p<0.01)
ALKBH5
YTHDC1
YTHDF2 (p<0.05)
IGF2BP2
METTL3
YTHDF3
METTL14
IGF2BP1 (p<0.05)
YTHDC2
IGF2BP3
HNRNPC
FTO
WTAP (p<0.01)
B
oeHAX-1
NC
shHAX-1
YTHDF1
YTHDF2
IGF2BP1
WTAP
HAX-1
GAPDH
60kDa
62kDa
63kDa
50kDa
35KDa
36KDa
C
Relative IGF2BP1 mRNA (%)
shHAX-1
NC
oeHAX-1
D
pcDNA3.1
oeHAX-1
Relative promtoer activity (%)
ns
pGL3-basic
pGL3-promoter
PRL-TK
E
Precursor IGF2BP1
Relative mRNA expression (%)
shHAX-1+Act-D
NC+Act-D
oeHAX-1+Act-D
Hours
F
Mature IGF2BP1
G
CHX
shHAX-1
oeHAX-1
IGF2BP1
GAPDH
70KDa
36KDa
IGF2BP1 expression levels
H
MG132
I
Time
0 2 4 6 8 12 Hours
shHAX-1+CHX
NC+CHX
oeHAX-1+CHX

◂**Figure 5** Regulation of IGF2BP1 mRNA stability and translation by IGF2BP1. **A** Differentially expressed m6A modifiers in cas9-HAX-1 and control cells determined by RNA-seq analysis. **B** WB analyses of YTHDF1, YTHDF2, IGF2BP1, and WTAP protein levels (GAPDH was used as the control). **C** RT-PCR analyses of IGF2BP1 mRNA level (GAPDH was used as the control). **D** Transfected cells with the pGL3-Basic-luc and pGL3-IGF2BP1-luc reporters and the pRL-TK plasmid for 24 h (data are presented as the ratio of the activity of the reporter plasmid to that of pRL-TK). **E** Precursor transcription inhibition subsequent to treatment with Act-D and **F** mature IGF2BP1 mRNA levels determined using RT-PCR. **G** IGF2BP1 levels in CNE-2 cells with HAX-1 knockdown or overexpression subjected to treatment with CHX or **H** MG-132 as determined by WB and quantitative analyses (GAPDH was used as the control). **I** IGF2BP1 expression in CNE-2 cells with HAX-1 knockdown or overexpression treated with CHX for the indicated time points as determined by WB and quantitative analyses (one-way ANOVA and two-way ANOVA). All data are presented as the mean ± SEM of at least three independent experiments. $*P < 0.05$, $**P < 0.01$, $***P < 0.001$, $****P < 0.0001$. *WB* western blot

Reagent or Resource	Source	Identifier
IGF2BP1	proteintech	22803-1-AP
NEDD4	proteintech	21698-1-AP
HA-Tag	Cell Signaling Technology	#3724
Myc-Tag	Cell Signaling Technology	#2276
YTHDF1	proteintech	17479-1-AP
YTHDF2	proteintech	24744-1-AP
WTAP	proteintech	60188-1-Ig
GAPDH	proteintech	10494-1-AP
Bacterial and Virus Strains		
lentiviral *HAX1*-shRNA	Shanghai Genechem	Target seq: GAGTGATGCAAGAAGTGAA
lentiviral *IGF2BP1*-shRNA	Shanghai Genechem	Target seq: ACAGTAGAGAACTGTGAGCAA
lentiviral *Rab7A*-shRNA	Shanghai Genechem	Target seq: gaAACAAGATTGACCTCGAAA
RFP-GFP-tagged LC3	Shanghai Genechem	tfLC3
Biological Samples		
Mouse tissues	This paper	N/A
Human NPC specimens	Affiliated Hospital of Nantong University	N/A
Chemicals, peptides, and recombinant proteins		
DMSO	Fisher Scientific	Cat#BP231-100
Cisplatin	Jiangsu HANSOH PHARMA	H20040813
Hochest	Thermo Fisher Scientific	62249
Propidium Iodide	Becton Dickinson and Company	556463
Fetal Bovine Serum	Biological Industries	04-001-1ACS
RPMI 1640	Biological Industries	01–100-1ACS
TRIzol reagent	BBI	B511311
Uranyl acetate	Polysciences, Hirschberg an der Bergstrasse, Germany	6159-44-0
Basic lead citrate	Sigma-Aldrich, Taufkirchen, Germany	15326
Actinomycin D	MCE, Sollentuna, Sweden	HY-17559
Cycloheximide	MCE, Sollentuna, Sweden	HY-12320
MG-132	MEC, Sollentuna, Sweden	HY-13259
AR6 buffer	AKOYA, Marlborough, Massachusetts, USA	AR600
CQ, chloroquine	MCE	HY-17589A
Critical commercial assays		
EdU cell proliferation assay	Shanghai Beyotime	C0078S
CCK8 kit	BBI	E606335
LIVE/DEAD viability kit	Shanghai Bestbio	BB-4126
BCA protein assay kit	Thermo Fisher Scientific	23227
Annexin V-FITC Apoptosis Detection Kit	Beyotime	C1063
Dual-Luciferase Reporter Assay Kit	Beyotime	RG088M
Oligonucleotides		
Primer1 for HAX1, Forward CAGGAGGAGGGATACGTTTCC	This paper	N/A
Primer1 for HAX1, Reverse CCCATATCGCTGAAGATGCTATT	This paper	N/A
Primer1 for pre-HAX1, Forward ATTACAGTCGCCTGCCAAAC	This paper	N/A
Primer1 for pre-HAX1, Reverse AGGTCAGGAGCTCAAAAGCA	This paper	N/A
Primer1 for IGF2BP1, Forward GCGGCCAGTTCTTGGTCAA	This paper	N/A
Primer1 for IGF2BP1, Reverse TTGGGCACCGAATGTTCAATC	This paper	N/A

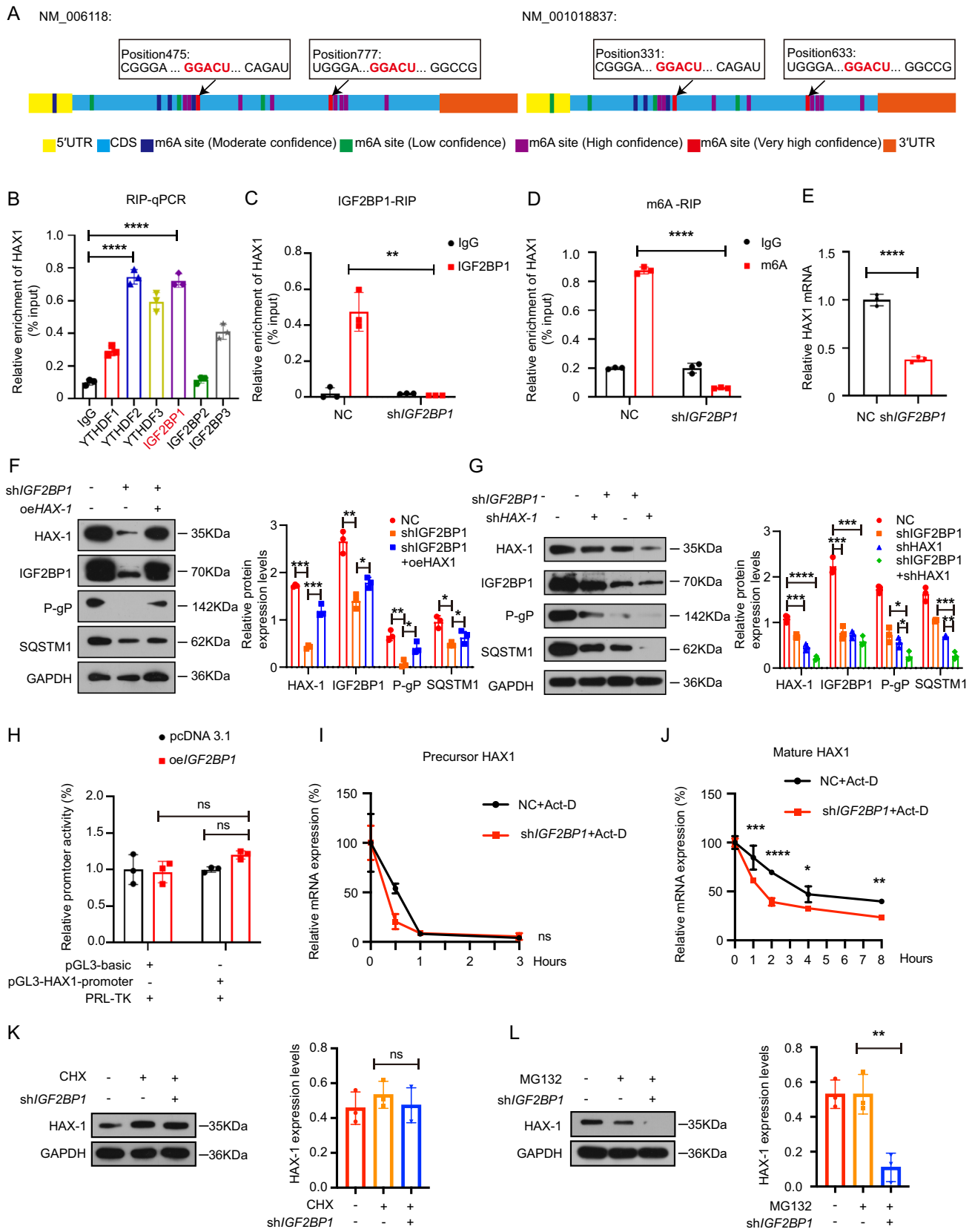
A
NM_006118:
Position475:
CGGGA ... GGACU... CAGAU
Position777:
UGGGA...GGACU... GGCCG
NM_001018837:
Position331:
CGGGA... GGACU... CAGAU
Position633:
UGGGA...GGACU... GGCCG
5'UTR
CDS
m6A site (Moderate confidence)
m6A site (Low confidence)
m6A site (High confidence)
m6A site (Very high confidence)
3'UTR
B
RIP-qPCR
Relative enrichment of HAX1 (% input)
IgG
YTHDF1
YTHDF2
YTHDF3
IGF2BP1
IGF2BP2
IGF2BP3
C
IGF2BP1-RIP
IgG
IGF2BP1
NC
shIGF2BP1
D
m6A -RIP
IgG
m6A
E
Relative HAX1 mRNA
F
shIGF2BP1
oeHAX-1
HAX-1
IGF2BP1
P-gP
SQSTM1
GAPDH
35KDa
70KDa
142KDa
62KDa
36KDa
Relative protein expression levels
NC
shIGF2BP1
shIGF2BP1 +oeHAX1
G
shHAX-1
shIGF2BP1
shHAX1
shIGF2BP1 +shHAX1
H
pcDNA 3.1
oeIGF2BP1
Relative promtoer activity (%)
ns
pGL3-basic
pGL3-HAX1-promoter
PRL-TK
I
Precursor HAX1
Relative mRNA expression (%)
NC+Act-D
shIGF2BP1+Act-D
Hours
J
Mature HAX1
K
CHX
HAX-1 expression levels
L
MG132

◂**Figure 6** IGF2BP1 regulates HAX-1 mRNA stability via m6A modification. **A** Schematic representation of m6A sites on HAX-1 mRNA. **B** Interaction of the m6A reader protein with HAX-1 mRNA as determined utilizing the RIP assay with anti-YTHDF1/2/3 and anti-IGF2BP1/2/3 antibodies. **C** Immunoprecipitated IGF2BP1 and RIP-qPCR was used to assess the interaction between the IGF2BP1 protein and HAX-1 mRNA in CNE-2 cells with IGF2BP1 knockdown. **D** Enrichment of HAX-1 in CNE-2 cells with IGF2BP1 knockdown as determined utilizing the RIP assay using anti-m6A antibodies. **E** Evaluation of HAX-1 mRNA using qRT-PCR. **F** WB analysis of HAX-1, IGF2BP1, P-gp, and SQSTM1 levels (GAPDH was used as the control). **G** WB analysis of HAX-1, IGF2BP1, P-gp, and SQSTM1 levels (GAPDH was used as the control). **H** Transfected cells with the pGL3-Basic-luc and pGL3-HAX1-luc reporters and pRL-TK plasmid with results presented as the ratio of the reporter plasmid activity to that of pRL-TK. **I** Precursor, after treatment with Act-D, and **J** mature HAX-1 mRNA **J** levels evaluated using RT-PCR. **K** HAX-1 levels in cells treated with CHX or **L** MG-132 determined using WB and quantitative analyses (GAPDH was used as the control, one-way ANOVA and two-way ANOVA). All data are presented as the mean ± SEM of at least three independent experiments. $*P < 0.05$, $**P < 0.01$, $***P < 0.001$, $****P < 0.0001$. *WB* western blot

Reagent or Resource	Source	Identifier
Primer1 for pre-IGF2BP1, Forward	This paper	N/A
TATTTGTGGAAAGGGGCAAG		
Primer1 for pre-IGF2BP1, Reverse	This paper	N/A
GCAAGCCACAGGATTAGAGC		
Primer1 for Rab7a, Forward	This paper	N/A
CAGTACAAAGCCACAATAGGAGC		
Primer1 for Rab7a, Reverse	This paper	N/A
CAAATACCAGAACGCAGCAGT		
Primer1 for GAPDH, Forward	This paper	N/A
GAACGGGAAGCTCACTGG		
Primer1 for GAPDH, Reverse	This paper	N/A
GCCTGCTTCACCACCTTCT		
siRNA target *NEDD4*_1	Guangzhou Ribobio	Target seq: GGAAGGACCTATTATGTAA
siRNA target *NEDD4*_2	Guangzhou Ribobio	Target seq: GGAACAACCTACACTTCCT
siRNA target *NEDD4*_3	Guangzhou Ribobio	Target seq: GGAGAATTATGGGTGTCAA
Deposited data		
RNA-seq data	This paper	GEO: https://www.ncbi.nlm.nih.gov/geo/query/acc.cgi?acc=GSE244097
Experimental models: cell lines		
Human: CNE-2	Gift of Musheng Zeng, Sun Yat-sen University Cancer Center	N/A
Human: CNE-2/DDP drug-resistant cell	ShangHAI AULU BioTECH	N/A
Software and algorithms		
GraphPad Prism	Graphpad Software	www.graphpad.com/scientific- software/prism/
ImageJ: Image processing and analysis	ImageJ	https://imagej.nih.gov/ij/ in Java
CellQuest acquisition and analysis programs	BD FACScan, Becton Dickinson and Company)	Version 0.9.13 alpha
X-tile Software	Yale School of Medicine; Rimm Lab	Version 3.6.1

Human NPC specimens

Tissue samples were collected from pathologically confirmed cases of NPC at the Affiliated Hospital of Nantong University, following approval by the ethics committee of the institution (IRB number: 2018-L049). Informed consent was obtained from all patients included in the study. Tissue microarrays to determine HAX1, IGF2BP1, and SQSTM1 expression levels were performed by Outdo Biotechnology (Shanghai, China). The X-tile bio-informatics tool for biomarker assessment and outcome-based cut-point optimization (version 3.6.1; Rimm Lab; Yale School of Medicine) was used to define low and high HAX1, IGF2BP1, and SQSTM1 expression levels, prior to performing survival analysis.

Cell culture

The CNE-2 cell line was gifted by Sun Yat-Sen University (Guangzhou, China) and cultured in RPMI 1640 medium (Biological Industries, Beit-Haeek, Israel; 01–100-1ACS) supplemented with 10 % fetal bovine serum (Biological Industries; 04-001-1ACS), as previously described [50]. Prior to use, short tandem repeat analysis was conducted to authenticate the CNE-2 cell line as well as routine tested for mycoplasma contamination.

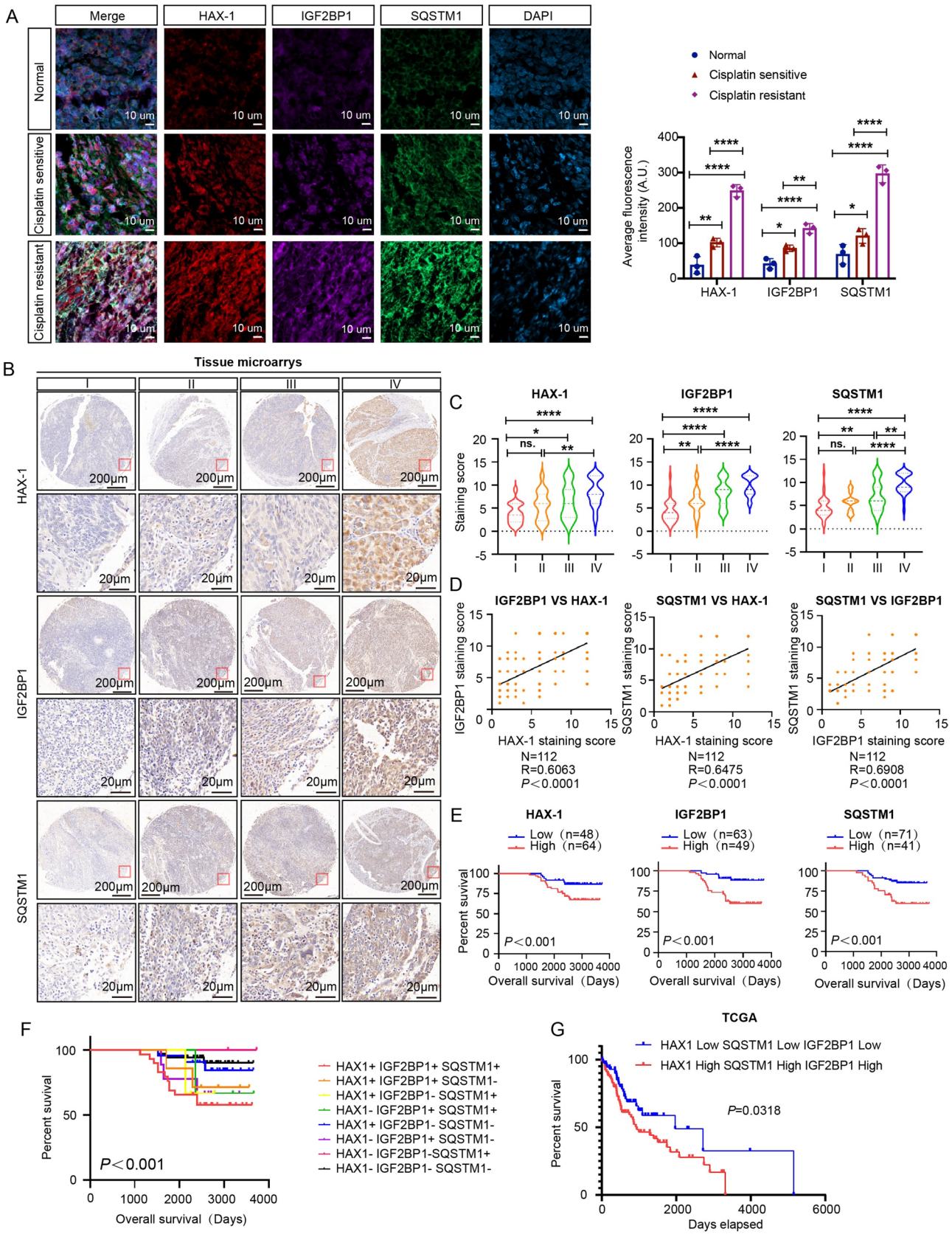
A
Merge
HAX-1
IGF2BP1
SQSTM1
DAPI
Normal
Cisplatin sensitive
Cisplatin resistant
10 um
Normal
Cisplatin sensitive
Cisplatin resistant
Average fluorescence intensity (A.U.)
HAX-1
IGF2BP1
SQSTM1
B
Tissue microarrys
I
II
III
IV
HAX-1
IGF2BP1
SQSTM1
200μm
20μm
C
HAX-1
IGF2BP1
SQSTM1
Staining score
ns.
D
IGF2BP1 VS HAX-1
SQSTM1 VS HAX-1
SQSTM1 VS IGF2BP1
HAX-1 staining score
IGF2BP1 staining score
SQSTM1 staining score
N=112
R=0.6063
P<0.0001
R=0.6475
P<0.0001
R=0.6908
P<0.0001
E
HAX-1
IGF2BP1
SQSTM1
Low (n=48)
High (n=64)
Low (n=63)
High (n=49)
Low (n=71)
High (n=41)
Percent suvival
P<0.001
Overall survival (Days)
F
Percent suvival
P<0.001
Overall survival (Days)
HAX1+ IGF2BP1+ SQSTM1+
HAX1+ IGF2BP1+ SQSTM1-
HAX1+ IGF2BP1- SQSTM1+
HAX1- IGF2BP1+ SQSTM1+
HAX1+ IGF2BP1- SQSTM1-
HAX1- IGF2BP1+ SQSTM1-
HAX1- IGF2BP1-SQSTM1+
HAX1- IGF2BP1- SQSTM1-
G
TCGA
HAX1 Low SQSTM1 Low IGF2BP1 Low
HAX1 High SQSTM1 High IGF2BP1 High
P=0.0318
Percent survival
Days elapsed

◂**Figure 7** Correlation between HAX-1, IGF2BP1, and SQSTM1 expression and their clinical significance in NPC. **A** Representative mIHC images of HAX-1, IGF2BP1, and SQSTM1 expression in chemoresistant NPC samples (n=3), chemosensitive NPC samples (n=3), and normal tissues (n=3). **B** Representative IHC staining of HAX-1, IGF2BP1, and SQSTM1 in NPC tissue microarrays (n=112). **C** Statistical comparison of HAX-1, IGF2BP1, and SQSTM1 expression across cancer clinical stages. **D** Correlation between HAX-1, IGF2BP1, and SQSTM1 levels in NPC tissues. **E** Kaplan-Meier analysis comparing overall survival based on HAX-1, IGF2BP1, and SQSTM1 expression levels (log-rank test). **F** Five-year OS curves for the low-risk, intermediate-risk, and high-risk DDP NPC chemoresistance groups. **G** Kaplan-Meier analysis of 5-year OS curves using the survival prediction model for DDP chemoresistance based on the co-analysis of HAX-1, IGF2BP1, and SQSTM1 levels in head and neck cancer from the TCGA database (one-way ANOVA). All data are presented as the mean ± SEM of at least three independent experiments. $^{*}P < 0.05$, $^{**}P < 0.01$, $^{****}P < 0.0001$

Immunofluorescence (IF), western blotting, and immunohistochemistry (IHC)

Western blotting, IF, and IHC assays were performed as previously [50] described using the antibodies listed in Table S2. Western blot images are shown in Fig. S7.

Transfection with plasmids and lentiviral vectors

Transfections were conducted following a previously described protocol [50]. Plasmids and lentiviral vectors, as well as their corresponding negative controls, were constructed and produced by GeneChem (Shanghai, China). Small interfering RNA (siRNA) and its corresponding negative controls were constructed and produced by Ribobio (Guangzhou, China). Autophagic flux was determined as previously described [35, 36] using tandem monomeric RFP-GFP-tagged LC3 (tfLC3) purchased from Genechem (Shanghai, China). The sequences of the short hairpin RNAs (shRNAs) and siRNAs used are listed in Table S3.

CRISPR-Cas9 assay

Guide RNA (sgRNA) preparation: sgRNA was designed using the CRISPR online tool (https://zlab.bio/guide-design-resources). The effective targeting site for *HAX-1* is 5′-GCTGAGGACTATGGAACCTT-3′.

Plasmid construction: the CRISPR-SaCas9-KKH system was selected as it allows for packaging and delivery through a single AAV vector and has known PAM sequences (50-NNNRRT-30) that are compatible with

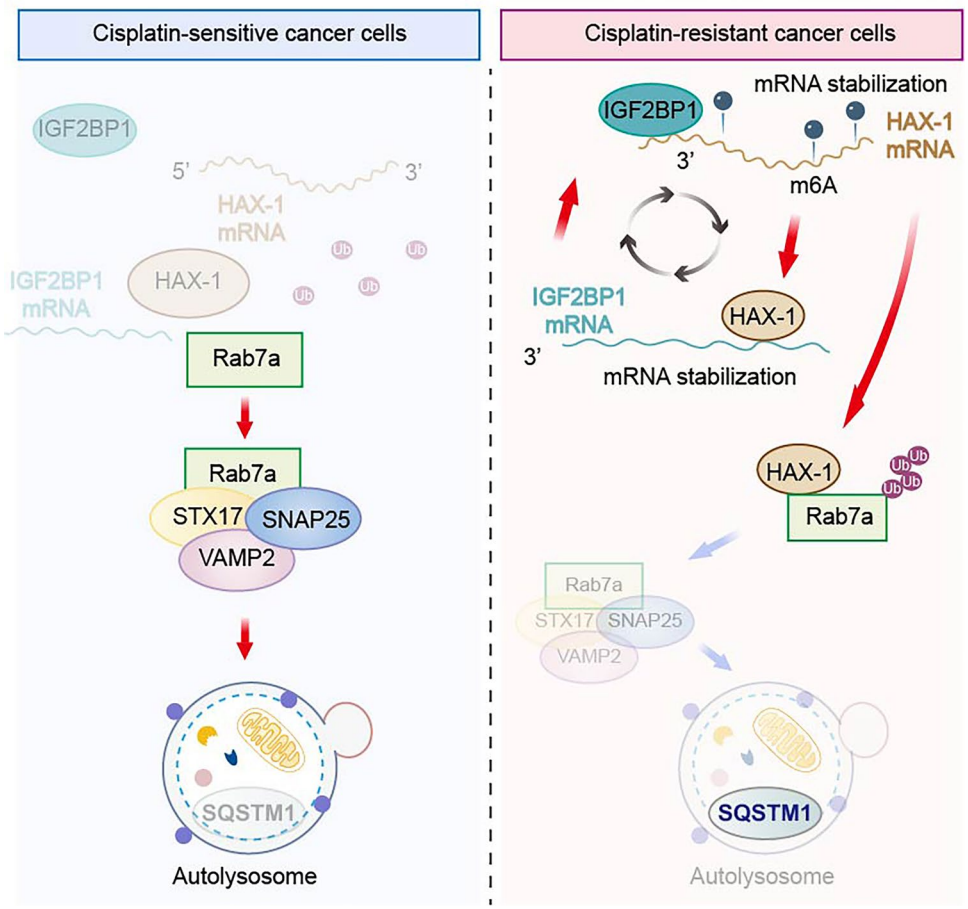

Figure 8 Schematic overview of the role of HAX-1 in DDP chemoresistance by effectively blocking autophagic flux in NPC. IGF2BP1 enhanced HAX-1 m6A methylation, thereby enhancing its stability. Furthermore, HAX-1 binds IGF2BP1 mRNA, thereby contributing to its stability and translation. Moreover, HAX-1 recruits NEDD4 to promote Rab7a degradation and inhibits binding of Rab7a with SNAREs by competitively binding to it, thereby blocking the fusion of autophagosomes with lysosomes

larger sgRNA numbers. sgRNA was inserted into the BsaI site of the pCMV_SaCas9-KKH_hU6 plasmid using PCR and Gibson assembly techniques. Finally, the plasmid was transfected into the cells for further validation and subsequent experiments.

qRT-PCR analysis

Total RNA was extracted using the TRIzol reagent (Invitrogen, USA) and reverse-transcribed. The SYBR Green PCR Master Mix (Roche, China, 04913914001) was used for qPCR amplification. Relative gene expression was calculated using the 2-ΔCT method. Relative mRNA expression levels were normalized to those of GAPDH. The primer sequences used are listed in Table S4.

EdU assay

The EdU cell proliferation assay was conducted using the BeyoClick™ EdU Cell Proliferation Kit (Shanghai Beyotime Co., Ltd., China, C0078S) as previously described [36].

Colony-forming assay

The colony-forming assay was performed as previously described [36]. Cells were plated at a density of 100 cells/mL in each well of a six-well plate, and 25 μg/mL of DDP was added once the cells had attached. The cells were then cultured for 2–3 weeks, after which the colonies were stained with hematoxylin and counted using ImageJ (NIH, USA).

Spheroid formation and LIVE/DEAD viability assay

Cells (20,000) were plated in PE 96-spheroid microwell plates, and 25 μg/mL DDP was added to them following spheroid formation. Cells were stained using the LIVE/DEAD® Viability/Cytotoxicity Kit (Shanghai Bestbio Co., Ltd., China, BB-4126) according to the manufacturer's instructions and images were captured using a fluorescence microscope (Zeiss, Göttingen, German, Axio Obse).

BALB/c nude mouse models

Six-week-old female BALB/c nude mice (Gempharmatech Co., Ltd) were used to construct tumor-bearing nude mouse models. Mice were randomly divided into groups (at least n = 6). NPC cells infected with lentiviruses were resuspended and 200 μL cell suspension (4×10^6 cells) was subcutaneously injected into the right forelimb armpits of the mice. DPP (Hansoh Pharma, Jiangsu, China) treatment commenced when the tumor sizes reached 0.125 cm^3.The mice were injected intraperitoneally with DPP (4 mg/kg) or an equivalent volume of PBS once every 2 days over 28 days. At the end of the treatment, the animals were sacrificed by asphyxiation with CO2. The tumors were excised, their weights and volumes were measured and were cryopreserved using liquid nitrogen.

Electron microscopic analysis

Cells were initially fixed, embedded, and sectioned. Ultrathin cell sections were subsequently stained with uranyl acetate (Polysciences, Hirschberg an der Bergstrasse, Germany, 6159-44-0) and basic lead citrate (Sigma-Aldrich, Taufkirchen, Germany, 15326). Finally, ultrathin sections of autophagosomes and autolysosomes were examined using a transmission electron microscope (JEOL Ltd., Tokyo, Japan, JEM-1230).

Co-Immunoprecipitation (Co-IP) assay

Cells were collected and lysed using pre-chilled IP lysis buffer with protein concentration determined using the BCA protein assay kit (Thermo Fisher Scientific, Waltham MA USA, 23227). Protein (1 mg) was incubated with antibodies at 4 °C overnight followed by 20 μL beads at 4 °C for 2 h. The bound protein complex was washed twice with IP lysis buffer and subjected to sodium dodecyl sulfate-polyacrylamide gel electrophoresis (SDS-PAGE). The antibodies were listed in Table S2. The 493 related proteins binding to HAX-1 are listed in Table S5.

RIP assay

Cells (2×10^7) were lysed using the RIP lysis buffer. Anti-target protein antibodies were immobilized on protein A/G magnetic beads and the magnetic bead-bound complex was separated using a magnet. Unbound substances were washed away and the final RIP assay results were obtained by real-time quantitative PCR following RNA extraction.

Flow cytometric analysis

Apoptosis assays were conducted using the Annexin V-FITC Apoptosis Detection Kit (Beyotime, Haimen, Jiangsu, China, C1063) as previously described [35, 50] with cells being analyzed by flow cytometry (Invitrogen, USA).

Establishment of DDP-resistant strains

CNE-2/DDP drug-resistant cell strains were purchased from ShangHAI AULU BioTECH (Shanghai, China) and

cultured at 37 °C, 5 % CO_2 and saturated humidity in the presence of DPP (1 μg/mL) to ensure drug resistance.

Luciferase reporter assay

The luciferase assay was performed using the Dual-Luciferase Reporter Assay Kit (RG088M; Beyotime, Haimen, Jiangsu, China) in order to measure promoter activation 24 h after transfection.

RNA stability assay

Cells were seeded in 6-well plates and treated with actinomycin D (MCE, Sollentuna, Sweden, HY-17559, 5 μg/mL) for 0, 2, 4, 6, 8, and 10 h. Equal numbers of cells were used for detecting mRNA expression levels using qRT-PCR. Relative abundance of mRNA at each time point was calculated with respect to that obtained at the baseline (0 h).

Protein stability assay

To inhibit translation, cycloheximide (CHX) (MCE, Sollentuna, Sweden, HY-12320, 0.2 mg/mL) was initially added to cells. Cell lysates were subsequently prepared at specific time points (0, 2, 4, 6, 8, and 10 h) and 20 μg of total extracted protein was subjected to western blotting to assess protein levels.

In-vitro ubiquitination assay

MG-132 (20 μM, HY-13259, MEC, Sollentuna, Sweden), an inhibitor of the ubiquitin-proteasome pathway, was added to the cells and incubated for 6 h followed by cell lysis to obtain total protein for western blotting.

Multiplex immunohistochemical (mIHC) analysis

Dewaxed and hydrated NPC tissue chips were placed in a repair solution and heated in a microwave oven for 15 min. This was followed by a 10-min sealing step using a blocking solution with the tissue chips incubated with the antibodies specific to the target proteins. Tissue sections were subjected to antigen repair by heating in a microwave using the AR6 buffer (AR600, AKOYA, Marlborough, Massachusetts, USA). The mIHC staining was performed following the addition of secondary antibodies, followed by heat induction and cooling for antigen repair with cell nuclei stained using DAPI. Finally, the slides were imaged using an automated quantitative pathology imaging system for biomarker positivity rate detection (PerkinELmer, Vectra 6-slide).

Statistical analysis

Statistical analyses were conducted using the Prism 6 (Boston, MA, USA) and SPSS 19.0 (IBM, USA) software packages. Experimental results were obtained from a minimum of three independent experiments and expressed as mean ± SD. Spearma''s rank correlation coefficient was used for correlation analysis. The two-tailed *t*-test and one-way ANOVA were used to determine statistical significance, with $*P < 0.05$, $**P < 0.01$, and $***P < 0.001$ considered statistically significant.

Supplementary Information The online version contains supplementary material available at https://doi.org/10.1007/s00018-025-05604-0.

Acknowledgments We sincerely appreciate Dr. Vangelis Kondylis (Institute of Pathology, University Hospital of Cologne) for his invaluable advice on this study.

Author contributions Conceptualization, B.Y. and Y.W.Y.; Methodology, B.Y., S.Y.Z., and M.G.; Investigation, B.Y., S.Y.Z., M.G., H.Y., S.P., H.J.X., W.H.C., S.G., Y.Z., Z.F.W, W.J.Z and B.Y.; Writing, B.Y. and S.G.; Funding Acquisition, Y.W.Y. and B.Y.; Resources, S.Y.Z and M.G; Supervision, B.Y. and Y.W.Y. Formal Analysis, B.Y. and S.Y.Z.

Funding This work was supported by grants from the National Natural Science Foundation of China (grant nos. 82372977, 82173288, 81972554, 82272839, and 82102701), Jiangsu Province Outstanding Youth Fund (BK20240127), Natural Science Foundation of Jiangsu Province (grant no. BK20201208), Jiangsu Provincial Medical Key Discipline (Laboratory) Cultivation Unit (grant no. JSDW202244), Jiangsu Provincial Research Hospital (grant no. YJXYY202204), CSCO Clinical Oncology Research Foundation of Beijing (grant no. Y-HR2019-0463).

Data availability The authors declare that all data supporting the findings of this study are available within the article and its Supplementary Material or contact the corresponding author upon reasonable request. The raw data of RNA-seq reported in this paper was submitted to GEO at: https://www.ncbi.nlm.nih.gov/geo/query/acc.cgi?acc=GSE244097.

Declarations

Conflict of interest The authors have no conflicts of interest to declare with regard to the publication of this manuscript.

Ethical approval This study was approved by the Affiliated Hospital of Nantong University, Jiangsu Province, China (IRB number: 2018-L049). The *in-vivo* experiments were approved by the Committee on the Ethics of Animal Experiments of Nantong University, Jiangsu Province, China (RDD number: 20180227-008). All mouse experiments were conducted according to NIH Guidelines and were approved by the Administration Committee of Experimental Animals, Jiangsu Province, China (Approval ID: SYXK (SU) 2007-0021).

Consent for publication Not applicable.

References

1. Ali S, Tahir M, Khan AA, Chen XC, Ling M, Huang Y (2019) Cisplatin synergistically enhances antitumor potency of conditionally replicating adenovirus via p53 dependent or independent pathways in human lung carcinoma. Int J Mol Sci 20(5):1125
2. Ernani V (2018) Nasopharyngeal carcinoma: chemotherapy or no chemotherapy? J Oncol Pract 14(10):607–608
3. Colevas AD, Yom SS, Pfister DG, Spencer S, Adelstein D, Adkins D, Brizel DM, Burtness B, Busse PM, Caudell JJ et al (2018) NCCN guidelines insights: head and neck cancers, version 1.2018. J Natl Compr Canc Netw 16(5):479–490
4. Li WF, Chen NY, Zhang N, Hu GQ, Xie FY, Sun Y, Chen XZ, Li JG, Zhu XD, Hu CS et al (2019) Concurrent chemoradiotherapy with/without induction chemotherapy in locoregionally advanced nasopharyngeal carcinoma: long-term results of phase 3 randomized controlled trial. Int J Cancer 145(1):295–305
5. Zhu QY, Zhao GX, Li Y, Talakatta G, Mai HQ, Le QT, Young LS, Zeng MS (2021) Advances in pathogenesis and precision medicine for nasopharyngeal carcinoma. MedComm 2(2):175–206
6. Guan S, Wei J, Huang L, Wu L (2020) Chemotherapy and chemo-resistance in nasopharyngeal carcinoma. Eur J Med Chem 207:112758
7. Wang N, Wang Z, Xu Z, Chen X, Zhu G (2018) A cisplatin-loaded immunochemotherapeutic nanohybrid bearing immune checkpoint inhibitors for enhanced cervical cancer therapy. Angew Chem Int Ed Engl 57(13):3426–3430
8. Xia Q, Ali S, Liu L, Li Y, Liu X, Zhang L, Dong L (2020) Role of ubiquitination in PTEN cellular homeostasis and its implications in GB drug resistance. Front Oncol 10:1569
9. Sakhawat A, Ma L, Muhammad T, Khan AA, Chen X, Huang Y (2019) A tumor targeting oncolytic adenovirus can improve therapeutic outcomes in chemotherapy resistant metastatic human breast carcinoma. Sci Rep 9(1):7504
10. Huang Z, Zhou L, Chen Z, Nice EC, Huang C (2016) Stress management by autophagy: implications for chemoresistance. Int J Cancer 139(1):23–32
11. Yu T, Guo F, Yu Y, Sun T, Ma D, Han J, Qian Y, Kryczek I, Sun D, Nagarsheth N et al (2017) Fusobacterium nucleatum promotes chemoresistance to colorectal cancer by modulating autophagy. Cell 170(3):548-563.e516
12. Zhu L, Zhu Y, Han S, Chen M, Song P, Dai D, Xu W, Jiang T, Feng L, Shin VY et al (2019) Impaired autophagic degradation of lncRNA ARHGAP5-AS1 promotes chemoresistance in gastric cancer. Cell Death Dis 10(6):383
13. Li X, He S, Ma B (2020) Autophagy and autophagy-related proteins in cancer. Mol Cancer 19(1):12
14. Smith AG, Macleod KF (2019) Autophagy, cancer stem cells and drug resistance. J Pathol 247(5):708–718
15. Levine B, Kroemer G (2019) Biological functions of autophagy genes: a disease perspective. Cell 176(1–2):11–42
16. Lotsberg ML, Wnuk-Lipinska K, Terry S, Tan TZ, Lu N, Trachsel-Moncho L, Rosland GV, Siraji MI, Hellesoy M, Rayford A et al (2020) AXL targeting abrogates autophagic flux and induces immunogenic cell death in drug-resistant cancer cells. J Thorac Oncol 15(6):973–999
17. Ferreira PMP, Sousa RWR, Ferreira JRO, Militao GCG, Bezerra DP (2021) Chloroquine and hydroxychloroquine in antitumor therapies based on autophagy-related mechanisms. Pharmacol Res 168:105582
18. Fadeel B, Grzybowska E (2009) HAX-1: a multifunctional protein with emerging roles in human disease. Biochim Biophys Acta 1790(10):1139–1148
19. Fan Y, Murgia M, Linder MI, Mizoguchi Y, Wang C, Lyszkiewicz M, Zietara N, Liu Y, Frenz S, Sciuccati G et al (2022) HAX1-dependent control of mitochondrial proteostasis governs neutrophil granulocyte differentiation. J Clin Invest 132(9):e153153
20. Simmen T (2011) Hax-1: a regulator of calcium signaling and apoptosis progression with multiple roles in human disease. Expert Opin Ther Targets 15(6):741–751
21. You B, Pan S, Gu M, Zhang K, Xia T, Zhang S, Chen W, Xie H, Fan Y, Yao H et al (2022) Extracellular vesicles rich in HAX1 promote angiogenesis by modulating ITGB6 translation. J Extracell Vesicles 11(5):e12221
22. You B, Cao X, Shao X, Ni H, Shi S, Shan Y, Gu Z, You Y (2016) Clinical and biological significance of HAX-1 overexpression in nasopharyngeal carcinoma. Oncotarget 7(11):12505–12524
23. Wang Z, Miao G, Xue X, Guo X, Yuan C, Wang Z, Zhang G, Chen Y, Feng D, Hu J et al (2016) The vici syndrome protein EPG5 is a Rab7 effector that determines the fusion specificity of autophagosomes with late endosomes/lysosomes. Mol Cell 63(5):781–795
24. Langemeyer L, Frohlich F, Ungermann C (2018) Rab GTPase function in endosome and lysosome biogenesis. Trends Cell Biol 28(11):957–970
25. Tian X, Teng J, Chen J (2021) New insights regarding SNARE proteins in autophagosome-lysosome fusion. Autophagy 17(10):2680–2688
26. Yap SV, Koontz JM (2011) Kontrogianni-Konstantopoulos A: HAX-1: a family of apoptotic regulators in health and disease. J Cell Physiol 226(11):2752–2761
27. Zaccara S, Ries RJ, Jaffrey SR (2019) Reading, writing and erasing mRNA methylation. Nat Rev Mol Cell Biol 20(10):608–624
28. Huang H, Weng H, Chen J (2020) m(6)A modification in coding and non-coding RNAs: roles and therapeutic implications in cancer. Cancer Cell 37(3):270–288
29. Zhuang H, Yu B, Tao D, Xu X, Xu Y, Wang J, Jiao Y, Wang L (2023) The role of m6A methylation in therapy resistance in cancer. Mol Cancer 22(1):91
30. Wu G, Zhou W, Pan X, Sun Y, Xu H, Shi P, Li J, Gao L, Tian X (2018) miR-100 reverses cisplatin resistance in breast cancer by suppressing HAX-1. Cell Physiol Biochem 47(5):2077–2087
31. Sun X, Li Y, Zheng M, Zuo W, Zheng W (2016) MicroRNA-223 increases the sensitivity of triple-negative breast cancer stem cells to TRAIL-induced apoptosis by targeting HAX-1. PLoS ONE 11(9):e0162754
32. Liu J, Tang Q, Li S, Yang X (2016) Inhibition of HAX-1 by miR-125a reverses cisplatin resistance in laryngeal cancer stem cells. Oncotarget 7(52):86446–86456
33. Li R, Zheng JZ, Huang X (2020) Suppression of HAX-1 induced by miR-325 resensitizes bladder cancer cells to cisplatin-induced apoptosis. Eur Rev Med Pharmacol Sci 24(18):9303–9314
34. Lin DC, Meng X, Hazawa M, Nagata Y, Varela AM, Xu L, Sato Y, Liu LZ, Ding LW, Sharma A et al (2014) The genomic landscape of nasopharyngeal carcinoma. Nat Genet 46(8):866–871
35. Zhu Q, Zhang Q, Gu M, Zhang K, Xia T, Zhang S, Chen W, Yin H, Yao H, Fan Y et al (2021) MIR106A-5p upregulation suppresses autophagy and accelerates malignant phenotype in nasopharyngeal carcinoma. Autophagy 17(7):1667–1683

36. You B, Zhang P, Gu M, Yin H, Fan Y, Yao H, Pan S, Xie H, Cheng T, Liu H et al (2022) Let-7i-5p promotes a malignant phenotype in nasopharyngeal carcinoma via inhibiting tumor-suppressive autophagy. Cancer Lett 531:14–26
37. Yang Q, Zhang MX, Zou X, Liu YP, You R, Yu T, Jiang R, Zhang YN, Cao JY, Hong MH et al (2018) A prognostic bio-model based on SQSTM1 and N-stage identifies nasopharyngeal carcinoma patients at high risk of metastasis for additional induction chemotherapy. Clin Cancer Res 24(3):648–658
38. Zhang R, Li SW, Liu L, Yang J, Huang G, Sang Y (2020) TRIM11 facilitates chemoresistance in nasopharyngeal carcinoma by activating the beta-catenin/ABCC9 axis via p62-selective autophagic degradation of Daple. Oncogenesis 9(5):45
39. Belizario JE, Alves J, Garay-Malpartida M, Occhiucci JM (2008) Coupling caspase cleavage and proteasomal degradation of proteins carrying PEST motif. Curr Protein Pept Sci 9(3):210–220
40. Ramakrishna S, Suresh B, Lim KH, Cha BH, Lee SH, Kim KS, Baek KH (2011) PEST motif sequence regulating human NANOG for proteasomal degradation. Stem Cells Dev 20(9):1511–1519
41. Toyofuku T, Morimoto K, Sasawatari S, Kumanogoh A (2015) Leucine-rich repeat kinase 1 regulates autophagy through turning on TBC1D2-dependent Rab7 inactivation. Mol Cell Biol 35(17):3044–3058
42. Numrich J, Peli-Gulli MP, Arlt H, Sardu A, Griffith J, Levine T, Engelbrecht-Vandre S, Reggiori F, De Virgilio C, Ungermann C (2015) The I-BAR protein Ivy1 is an effector of the Rab7 GTPase Ypt7 involved in vacuole membrane homeostasis. J Cell Sci 128(13):2278–2292
43. Li ZX, Zheng ZQ, Yang PY, Lin L, Zhou GQ, Lv JW, Zhang LL, Chen F, Li YQ, Wu CF et al (2022) WTAP-mediated m(6)A modification of lncRNA DIAPH1-AS1 enhances its stability to facilitate nasopharyngeal carcinoma growth and metastasis. Cell Death Differ 29(6):1137–1151
44. Chen B, Huang Y, He S, Yu P, Wu L, Peng H (2023) N(6)-methyladenosine modification in 18S rRNA promotes tumorigenesis and chemoresistance via HSF4b/HSP90B1/mutant p53 axis. Cell Chem Biol 30(2):144-158.e110
45. Zheng ZQ, Huang ZH, Liang YL, Zheng WH, Xu C, Li ZX, Liu N, Yang PY, Li YQ, Ma J et al (2023) VIRMA promotes nasopharyngeal carcinoma, tumorigenesis, and metastasis by upregulation of E2F7 in an m6A-dependent manner. J Biol Chem 299(5):104677
46. Zhang P, He Q, Lei Y, Li Y, Wen X, Hong M, Zhang J, Ren X, Wang Y, Yang X et al (2018) m(6)A-mediated ZNF750 repression facilitates nasopharyngeal carcinoma progression. Cell Death Dis 9(12):1169
47. Zhao Y, Huang S, Tan X, Long L, He Q, Liang X, Bai J, Li Q, Lin J, Li Y et al (2022) N(6) -Methyladenosine-modified CBX1 regulates nasopharyngeal carcinoma progression through heterochromatin formation and STAT1 activation. Adv Sci (Weinh) 9(36):e2205091
48. Zheng ZQ, Li ZX, Zhou GQ, Lin L, Zhang LL, Lv JW, Huang XD, Liu RQ, Chen F, He XJ et al (2019) Long noncoding RNA FAM225A promotes nasopharyngeal carcinoma tumorigenesis and metastasis by acting as ceRNA to sponge miR-590-3p/miR-1275 and upregulate ITGB3. Cancer Res 79(18):4612–4626
49. Wang YQ, Wu DH, Wei D, Shen JY, Huang ZW, Liang XY, Cho WCS, Ma J, Lv J, Chen YP (2023) TEAD4 is a master regulator of high-risk nasopharyngeal carcinoma. Sci Adv 9(1):eadd0960
50. You B, Xia T, Gu M, Zhang Z, Zhang Q, Shen J, Fan Y, Yao H, Pan S, Lu Y et al (2022) AMPK-mTOR-mediated activation of autophagy promotes formation of dormant polyploid giant cancer cells. Cancer Res 82(5):846–858